# Advances in High-Resolution Microscopy for the Study of Intracellular Interactions with Biomaterials

Catherine S. Hansel[1,2], Margaret N. Holme[3], Sahana Gopal[1,4], Molly M. Stevens[1,3*]

[1]Department of Materials, Department of Bioengineering and Institute for Biomedical Engineering, Imperial College London, London, UK
[2]Department of Chemistry, Imperial College London, London, UK
[3]Department of Medical Biochemistry and Biophysics, Karolinska Institute, Stockholm, Sweden
[4]Department of Medicine, Imperial College London, London, UK

ORCIDs
C.S.H.: 0000-0002-2525-1856
M.N.H.: 0000-0002-7314-9493
M.M.S.: 0000-0002-7335-266X

Correspondence to:

* E-mail: m.stevens@imperial.ac.uk

Molly M. Stevens, PhD
Department of Materials
Imperial College London
Prince Consort Road
SW7 2AZ
London, United Kingdom

## Abstract

The study of sophisticated biomaterials and their cellular targets requires visualization methods with exquisite spatial and temporal resolution to discern cell organelles and molecular events. Monitoring cell-material interactions at high resolution is key for the continued development and optimization of biomaterials, for monitoring cell uptake of cargo, and for understanding the cell response to extracellular cues. This review evaluates the advantages and disadvantages of different forms of electron microscopy and super-resolution microscopy in elucidating how biomaterial surface chemistry and topography can affect intracellular events at the nanoscale.

## Keywords

Super-resolution microscopy, electron microscopy, cell-material interactions

## Glossary of super-resolution microscopy terms

| | |
|---|---|
| AFM | Atomic force microscopy |
| CLEM | Correlative light and electron microscopy |
| DyMIN | Dynamic intensity minimum |
| EELS | Electron energy loss spectroscopy |
| EM | Electron microscopy |
| ET | Electron tomography |
| EDX | Energy dispersive X-ray spectroscopy |
| FIB-SEM | Focused ion beam scanning electron microscopy |
| FLM | Fluorescent light microscopy |
| FRET | Fluorescence resonance energy transfer |
| LLSM | Lattice light sheet microscopy |
| LSM | Light sheet microscopy |
| MPM | Multiphoton microscopy |
| PAINT | Points accumulation for imaging in nanoscale topography |
| PALM | Photoactivation localization microscopy |
| SEM | Scanning electron microscopy |
| SICM | Scanning ion conductance microscopy |
| SIM | Structured illumination microscopy |
| SMLM | Single molecule localization microscopy |
| SRM | Super-resolution microscopy |
| STED | Stimulated emission depletion |
| STEM | Scanning transmission electron microscopy |
| STORM | Stochastic optical reconstruction microscopy |
| TEM | Transmission electron microscopy |
| TIRF | Total internal reflection fluorescent |

## Introduction

Cells are continually interacting with a dynamic external environment *in vivo*. This environment consists of an extracellular matrix (ECM) which is composed of a variety of proteins and polysaccharides organized into unique compositions and topographies, reflecting the requirements for a particular tissue. The cells deposit, maintain and remodel the ECM and in return, the ECM interacts with receptor-protein complexes such as transmembrane integrins, inducing biochemical and mechanical signaling cascades involving structures such as focal adhesion (FA) complexes, the actomyosin cytoskeleton, and the nucleus. The topographical and chemical cues presented by the ECM can influence many cellular functions such as cell survival, proliferation, and differentiation [1]. This realization has led to the development of biomaterials with unique nanotopographies and surface-properties in order to precisely manipulate cell behavior [2–4]. For example, a variety of cell substrates with nanotopographical cues have been designed which present various micro-/nano-topograhies [5–11], stiffnesses [12–15], and spatial confinements [16–24], and developments in chemistry have enabled the tethering of chemically functional groups [25–27], ECM constituents [28,29], growth factors [30] and cell surface ligands [31,32] to biomaterials in order to control cell fate. Nanotopography and surface chemistry have also been exploited in the development of biomaterials for intracellular delivery, increasing the frequency of endocytotic events [33–39] (**Figure 1**).

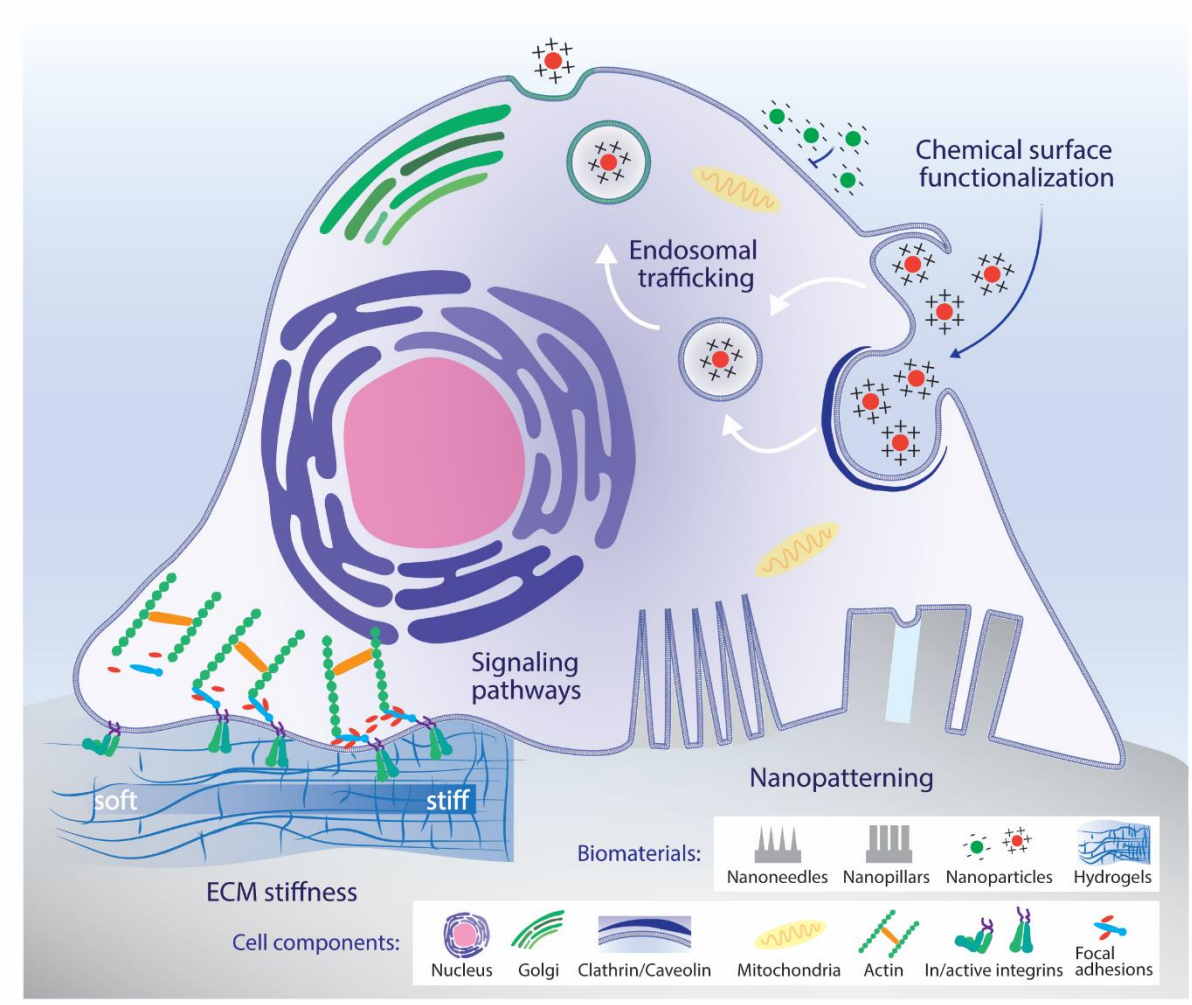


*Figure 1: Summary schematic of a cell interacting with various biomaterials. Biomaterials with engineered nanotopographies, stiffnesses and chemical functionalizations can be utilized to direct cell fate and function. When going from a soft to stiff hydrogel, integrins are activated, focal adhesions are formed and cells spread, showing increased actin/cytoskeletal tension. The surface functionalization and nanotopography of a biomaterial can also affect cell adhesion and can help mediate biomaterial entry into the cell.*

Scanning probe microscopy techniques such as atomic force microscopy (AFM), scanning ion conductance microscopy (SICM), and scanning electron microscopy (SEM) have been highly effective at imaging extracellular biointerfaces at the nanoscale, demonstrating the impact of nanotopography on cell behavior [40–42]. However, the mechanisms that are involved in the cellular response to nanotopography, and the effect of surface chemistry on the cell, are less well studied. Therefore, signaling pathways and intracellular events that lead to changes in cell behavior following cellular interfacing with materials must be further evaluated. High-resolution imaging techniques that can image multiple specific proteins with respect to cellular compartments in 3D, as well as the nanoscale architecture of a biomaterial, will be critical in elucidating the signaling pathways that are activated in response to precise environments within biomaterials. Moreover, since the cell response can be transient in nature, live-imaging techniques with minimal toxic effects will also be crucial for the development of new and improved biomaterials **(Figure 2)**.

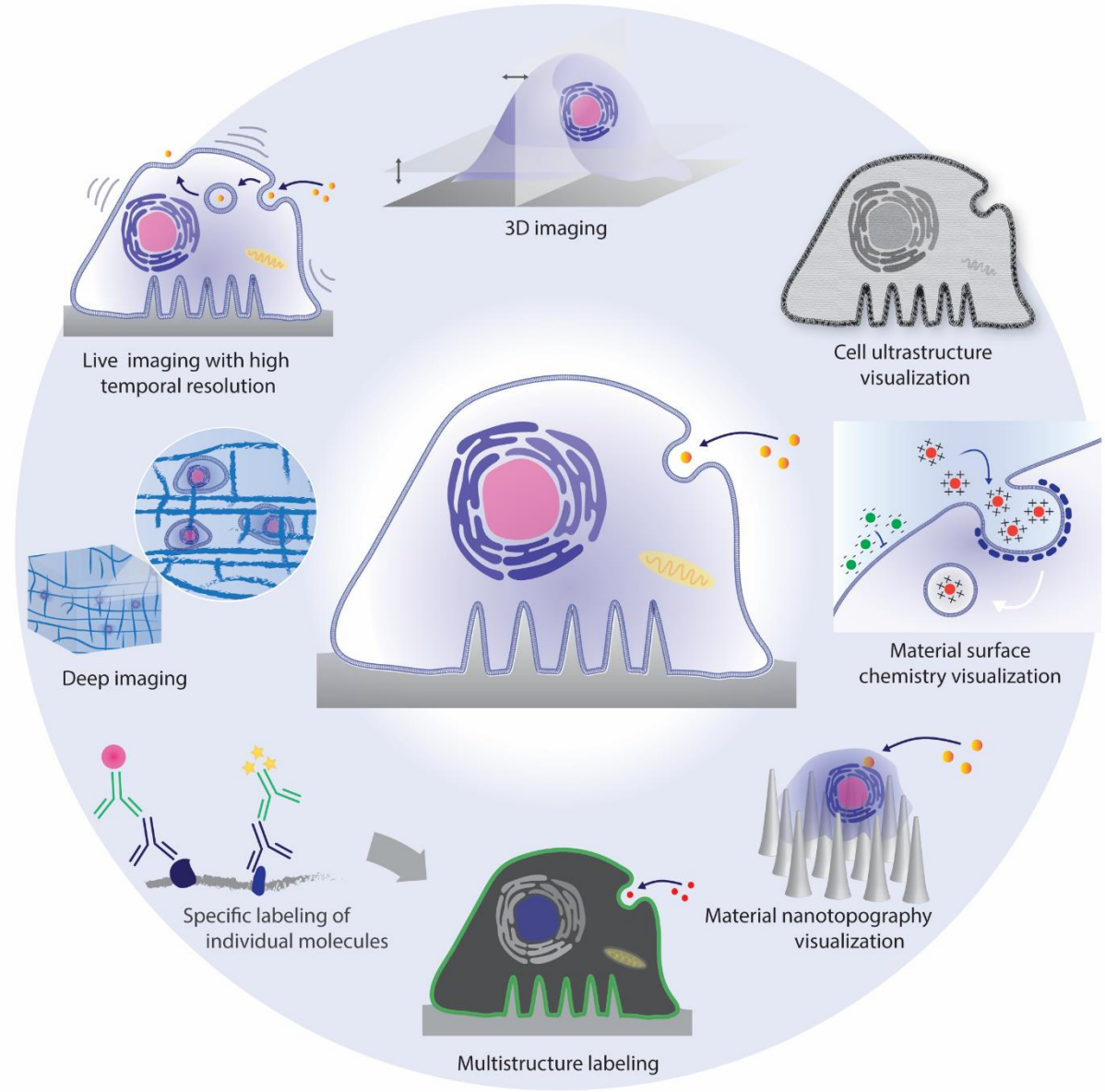


*Figure 2: The ideal high-resolution imaging technique for cell-material interactions. Summary of the key properties of an imaging system for cell-material interactions using an example of a cell interfacing with a vertical array of nanostructures and taking up nanoparticles.*

Commercial (e.g. Volocity, Amira and Imaris) and open-source (e.g. Fiji/ImageJ [43,44], CellProfiler [45], Icy [46], and V3D [47]) software packages have been developed to enable the processing and analysis of microscopy images. In addition, programming languages (e.g. Matlab, Python, and R) are useful for customized analyses and machine learning. Although most heavily developed for the quantification of phenotypes in lower-resolution images and high throughput experiments [48], these software packages and programming languages will be highly useful in the assessment and quantification of high-resolution interactions between cells and materials. In this review we will present the advantages and disadvantages of electron microscopy (EM) (specifically transmission EM (TEM), and focused ion beam SEM (FIB-SEM)) and super-resolution microscopy (SRM) techniques (specifically structured illumination microscopy (SIM), stimulated emission depletion (STED)

microscopy and single molecule localization microscopy (SMLM)) for the visualization of cell-material interactions at the molecular level.

## Electron microscopy and intracellular cell-material interactions

Electron microscopy has been used to visualize the interactions between cells and a wide range of biomaterials at the intracellular level. Electron microscopes use a beam of accelerated electrons as the illumination source, whose path is controlled by electromagnetic and/or electrostatic lenses. This gives EM a more powerful resolving power than light microscopy since electrons have a shorter wavelength than photons. This review will focus on TEM and FIB-SEM applications for cell-material interactions, with a focus on sample preparation and the reduction of artefacts.

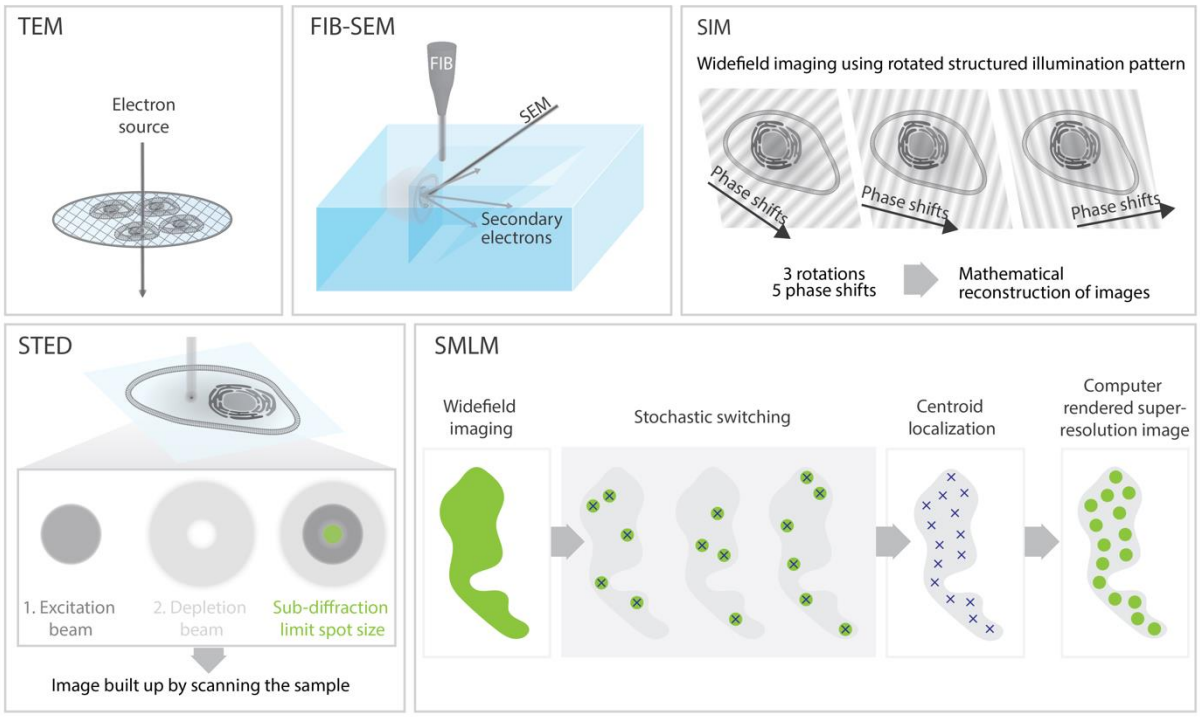


*Figure 3: Diagrams of high-resolution microscopy techniques for intracellular biomaterial interactions. Top left, schematic of transmission electron microscopy (TEM): An electron beam is accelerated through an electromagnetic field that narrowly focusses the beam. The beam passes through a very thin slice of sample material (less than 100 nm). The electrons that pass through the sample hit a detector and produce an image. The image is brighter where the sample has less density as more electrons get through. Top middle, schematic of focused ion beam scanning electron microscopy (FIB-SEM): A focused Gallium ion beam orthogonally mills a sample embedded in contrasted resin. Whilst this milling is underway, angled scanning electron microscopy (SEM) is used to image the front face of the sample, enabling a 3D reconstruction of the sample to be built up. Top right, schematic of structured illumination microscopy (SIM): A series of images are captured using a patterned excitation beam that is rotated in steps and phase shifted. In each individual image, the interaction of the patterned excitation beam with the sample leads to Moiré patterns that contain high frequency information. The image stacks can be reconstructed in reciprocal space to obtain images with a 2-fold resolution improvement versus wide-field microscopy. Bottom left, schematic of stimulated emission depletion (STED) microscopy: STED microscopy uses the same approach as a laser scanning confocal microscope but achieves higher resolution by reducing the size of the point spread function (PSF) by stimulated emission. A donut shaped "STED" laser that overlaps with the excitation beam is pulsed shortly after*

*the normal excitation laser pulse. The STED beam instantaneously 'bleaches' excited fluorophores back to their ground state by stimulated emission before spontaneous fluorescence emission can occur. Therefore, only the molecules in the center of the STED beam fluoresce, the PSF is reduced, and resolution is increased. Bottom right, schematic of single molecule localization microscopy (SMLM): SMLM techniques ensure that only a small, random subpopulation of fluorophores are switched on and recorded at any given time so that neighboring fluorophores within the same point spread function (PSF) can be isolated and imaged separately at sub-diffraction precision. This process of fluorophore activation and inactivation is repeated over a high number of frames to ensure all the fluorophores are imaged. The resulting frames are then merged by post-processing to create a final image.*

## Transmission electron microscopy (TEM) for cell-ultrastructure and biomaterial visualization in 2D

In TEM, an electron beam is transmitted through a very thin sample that is semi-transparent to electrons (**Figure 3**). The transmitted electrons are then focused to form an image on the detector, which is typically a charge-coupled device (CCD) camera. Recently, the development of direct electron detectors has seen a huge improvement in electron sensitivity and TEM can image samples at near-atomic level with a very limited dose of electrons [49]. TEM has been used to assess the interaction between the ultrastructure of cells and a variety of materials such as hydrogels [50,51], implant materials [52], biosensing apparatus [53], nanopillars and nanoneedles [37,38,54], and electrical devices [55]. For example, it has been used to quantify the effect of surface roughness on cell contact in titanium implants (**Figure 4a**) [52], cell engulfment of microelectrodes (**Figure 4b**) [55], and how membrane continuity is maintained around nanoneedles/nanopillars with nm-scale precision (**Figure 4c**) [37,38,54]. These findings have provided insight into intracellular interactions at the cell-material interface, where the material's nanotopography can be imaged without the need for labelling.

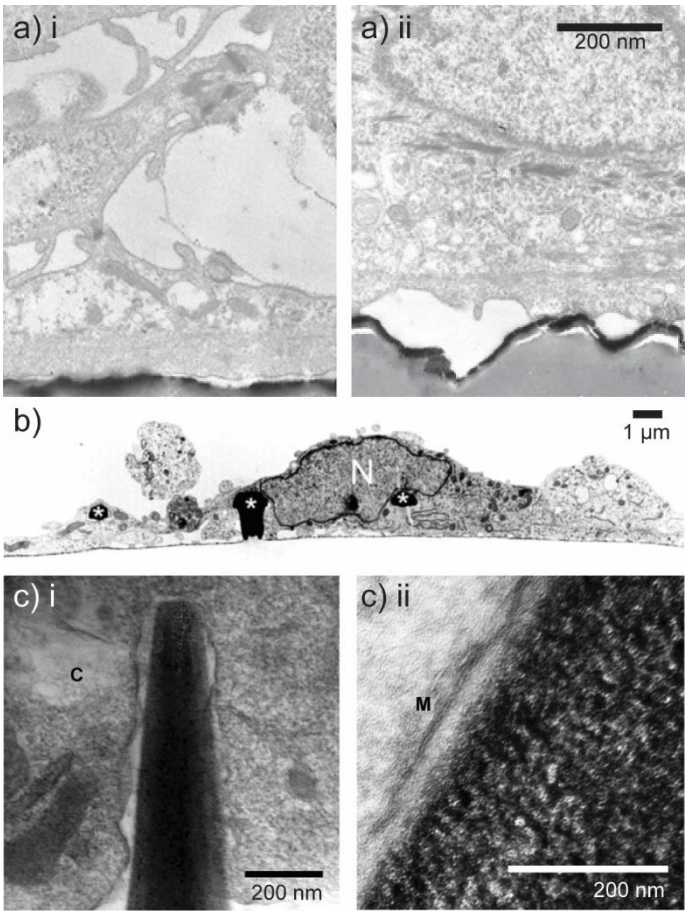


*Figure 4: Selected examples of transmission electron microscopy (TEM) applied to visualize cell-material interactions. a) TEM evaluation of the surface proximity between the cell membrane and a titanium implant surface. Cell contact with the surface was most frequently found on protruding portions of rough surfaces. Adapted from Baharloo et al., J. Biomed. Mater. Res. - Part A 74, 12–22, 2005* [52] *with permission from John Wiley and Sons, copyright 2005. b) TEM used to show the engulfment of ~1 µm size gold mushroom-shaped microelectrodes (gMµE, marked by asterisks) by neurons. Adapted from Fendyur et al. Front. Neuroeng. 4, 1-14, 2011* [55]*, open-access article. c) i) front and ii) side-view TEM imaging of a focused ion beam (FIB) lift-out thin section of a cell-nanoneedle interface. C = cytosol, M = membrane. Adapted from Gopal et al. Advanced Materials. 9, 1806788, 2019* [37]*, with permission from John Wiley and Sons, copyright 2019.*

Although the resolution of TEM enables the ultrastructure of cells and biomaterials to be resolved, further interpretation is required in order to gain information on the localization of chemistry within the sample. Spectroscopic techniques such as energy filtered TEM or scanning TEM (STEM) in conjunction with electron energy loss spectroscopy (EELS) [56] can provide information about the spatial resolution of specific elements in biological samples [57]. EELS in combination with electron tomography has also been reported to study osseointegration of titanium implants [58]. More generally, combinations of fixing and staining methods can be used to determine the exact nature and localization of intracellular components. Typically, stains are mixed with fixatives such as glutaraldehyde. One of the most common stains is osmium tetroxide which heavily stains lipids, and improves the contrast of membranous structures within the cell [59]. However, lipid staining is often insufficient for the visualization of structures with high nucleic acid or protein content, such as chromatin and protein complexes. These structures require contrast agents such as uranyl acetate [60] which binds to nucleic acids, glycoproteins and lipids. Immunogold staining using antibody-labeled gold

nanoparticles is also a widely explored technique for visualizing and quantifying specific markers within the cell [61,62].

Cryo-TEM allows samples to be imaged in vitrified ice in their near-native hydration states without the need for staining, avoiding artefacts caused by chemical fixation and dehydration steps usually required for conventional TEM [49]. The development of cryo-TEM techniques, where aqueous samples are blotted on a TEM grid then immediately vitrified (typically in liquid ethane) [49,63], won the Nobel Prize for Chemistry in 2017. A low dose of electrons (usually <10-20 e/A^2) is used to preserve the high-resolution information of biological samples. Near atomic resolution is still achieved at this limited dose due to the development of direct electron detectors, which dramatically improve the sensitivity of the detector. In low dose mode operation, regions of interest on the grid are typically identified at low magnifications and focusing occurs in areas of the sample adjacent to the region of interest to avoid unwanted pre-exposure of the sample. Therefore, the imaged area is only exposed to appreciable electron dose during image acquisition [49].

TEM requires ultra-thin sample sections (< 100 nm) to avoid unwanted plural scattering. In the case of larger structures such as cells, obtaining ultra-thin samples requires a number of costly and lengthy processing steps that prevent the imaging of live samples and produce a number of artefacts. Vitrification by high pressure freezing, usually in the presence of a cryo-protectant, allows access to thicker vitrified samples which can then be sectioned to samples thin enough for imaging by TEM in cryo-conditions [64]. Alternatively, samples can be fixed, dehydrated and block embedded in resin prior to staining to enable sectioning with an ultra-microtome. However, the mechanical sectioning of samples with different densities (e.g. cell and substrate) can generate high processing artefacts, and it is not usually possible to section hard substrates such as metals [65]. Focused ion beam (FIB) lift out preparation techniques largely overcome these problems, where samples are milled using the FIB to the required thickness for imaging by TEM [37,66,67]

Since TEM samples are ultra-thin, it is largely considered a 2D microscopy technique, although 3D images can be obtained by electron tomography (ET), which uses a fixed beam and rotates a sample of up to 500 nm thickness through various angles to generate a 3D image [64]. ET of fixed samples and cryo-ET of intact cells allows different parts of the cell to be extracted by applying segmentation and template matching software to the tomogram images [64,68]. The resulting extracted 3D volumes can be visualized and quantified. The recently developed technique of subtomogram averaging allows higher resolution information about the structures of particles (i.e. protein and protein complex structures, and their dynamics) to be obtained [49,64]. Here, sub-nm resolution in 3D [69] can be achieved by averaging 3D volumes or “subtomograms” of individual particles extracted from the tomograms. Wedge artifacts which arise in ET due to the limited tilt angle are also mitigated since the particles are randomly oriented within the sample [49]. Sections up to 1 µm thick can be imaged using STEM [70] and cryo-STEM [71] by detecting the angles of scattered electrons. Software packages such as Amira (from Visage Imaging) use guided segmentation to create 3D models of cells that can be segmented to show different ultrastructures, e.g. a human erythrocyte infected with *P. falciparum*, with spatial resolution down to 5-10 nm [70]. However, cells are generally larger than 1 µm and thus whole cell information cannot be obtained from STEM and cryo-STEM. Dynamic information on the cell-material interface is not easily accessible via TEM. Liquid TEM cells are available and have been successfully used to characterize particle growth [72,73]. However, although live-cell EM on cells in their native liquid environment has been published, this technique is limited as the electron beam exposure required for imaging is toxic to cells [74].

## Focused ion beam scanning electron microscopy (FIB-SEM) for cell-ultrastructure and biomaterial visualization in 3D

Focused ion beam scanning electron microscopy provides a solution for the high processing artefacts induced by sample sectioning in TEM whilst enabling 3D imaging of whole cells [75]. Instead of using mechanical sectioning as in TEM, resin embedded samples are directly introduced under a focused ion beam (FIB). The FIB is used to mill the front face of the sample to obtain serial cross-sections and these cross-sections are imaged *via* SEM in a process commonly known as slice and view **(Figure 3)**. A SEM raster scans the surface of a sample with a beam of electrons, producing secondary, back-scattered and Auger electrons that are collected by a detector to give an image displaying the surface topography of a sample. In the case of FIB-SEM, this allows the visualization of sub-cellular structures over hundreds of sections per cell to produce a complete 3D reconstruction of the cell's ultrastructure. A drawback of FIB-SEM is that the samples still require contrast enhancing methods similar to those used for TEM, and FIB-SEM is unable to image cells live.

Focused ion beam scanning electron microscopy has been employed to study cell interactions with biomaterials such as pillars [76,77], wires [38,78,79], scaffolds [80] and 3D gel systems [81]. For example, image quantification of FIB-SEM images has shown that the cell membrane tightly interfaces with protruding structures but minimally interfaces with invaginating structures (**Figure 5a**) [76]. Moreover, FIB-SEM has been used to demonstrate that porous silicon nanoneedles tightly interface with cells and can deliver quantum dots into the cell interior (**Figure 5b**) [38]. This enhanced biomolecule delivery is likely due to the clathrin pits and caveolae endocytic vesicles which accumulate around the nanoneedles (**Figure 5c**) [37]. Amira software is particularly useful for 3D and 4D data visualization of FIB-SEM images, marking specific structures and regions of interest in 3D image volumes which can then be quantified by software such as Fiji or Volocity. For example, Amira software has been used to segment nanoneedles, the cell membrane and the nuclear envelope in a 3D image of nanoneedles interacting with a cell; thus enabling the quantification of the depth of nanoneedle cytosolic interfacing and the distance of the nanoneedles from the nucleus [38].

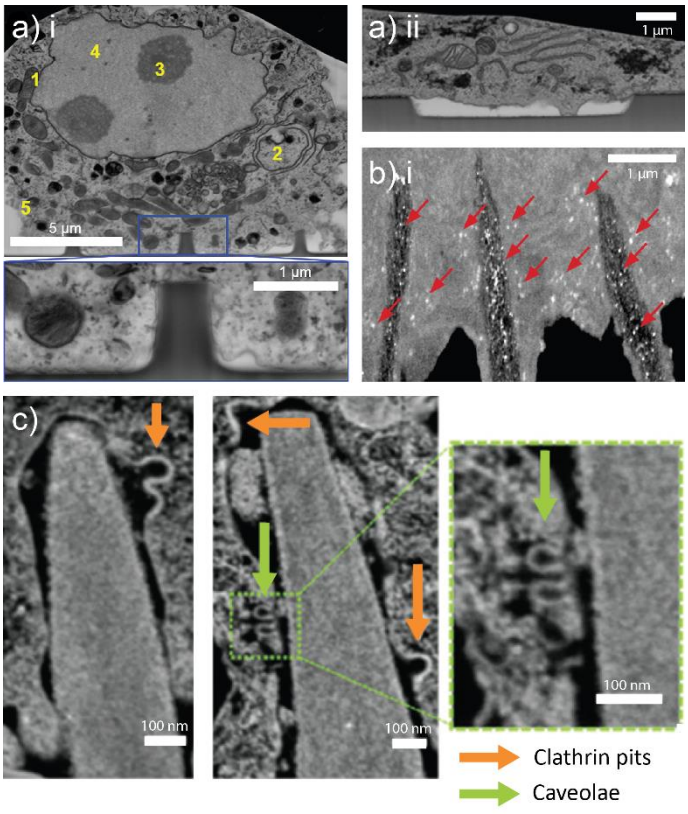

*Figure 5: Selected examples of focused ion beam scanning electron microscopy (FIB-SEM) applied to visualize cell-material interactions. a) FIB-SEM to show that the cell membrane tightly interfaces with nanoscale protruding structures, but barely deforms outwards to interface with invaginating structures. Adapted from Santoro et al., ACS Nano, 11(8), 8320–8328, 2017* [76]*, with permission from the American Chemical Society, copyright 2017. b) FIB-SEM cross sections of cells injected with quantum dots through tight interfacing with quantum dot adsorbed nanoneedles. Adapted from Chiappini et al., ACS Nano, 9, 5500-5509, 2015* [38]*, with permission from the American Chemical Society, copyright 2015. c) FIB-SEM image of a cell-nanoneedle interface with endocytotic vesicles (clathrin pits and caveolae) accumulating around the nanoneedles. Adapted from Gopal et al. Advanced Materials. 9, 1806788, 2019* [37]*, with permission from John Wiley and Sons, copyright 2019.*

### Intracellular labelling for electron microscopy

It is possible to combine EM with intracellular labelling [82,83], which would enable the precise localization of cellular targets with respect to the cell ultrastructure and the geometry of a material. Since the electron microscope is unable to visualize fluorescent probes, antibodies are instead conjugated to colloidal gold particles (immunogold) in order to visualize labelled intracellular structures with TEM, and these can also be utilized in FIB-SEM [62]. Labelling can be carried out prior to heavy metal staining and resin embedding (pre-embedding) or after preparation of ultra-thin sections (post-embedding). Pre-embedding labelling achieves greater specificity and labelling densities than post-embedding labelling [84], however it often requires permeabilization of the cell in order for the immunogold to penetrate into the cell, which can damage cellular ultrastructure and disrupt certain receptor-protein complexes at the cell surface [85]. Methods have been established to circumvent these issues with penetration, for example extremely small gold particles (1.4 nm) can be conjugated to antibodies [86], and gentler permeabilization methods have been adopted [62]. Recently, immunogold FIB-SEM has demonstrated simultaneous spatial mapping of cellular ultrastructure and biomolecular information in different cell-material systems [62]. For example, the volumetric distribution of an epigenetic marker H3K9me3 in the nucleus of a neural stem cell subjected to flat substrates or 10 µm microgrooves was assessed and quantified at nm separation distances. Further methods to circumvent penetration issues include genetically encoded EM tags that generate strong EM contrast [87]. Example tags include horseradish peroxidase (HRP) and enhanced ascorbate peroxidase (APEX) [88,89]. However, these methods have a number of drawbacks. For example, it is hard to express HRP in the cytosol of mammalian cells since HRP requires higher than physiological levels of intracellular calcium concentrations for binding [90]. Moreover, genetic tags might affect endogenous protein function and localization, and can be sensitive to different cell types [87]. Finally, the genetic tags require enhanced contrast *via* diaminobenzidine (DAB), and the fixation and incubation with DAB reagents must be carefully controlled so that they are localized to the specific subcellular target of interest [88]. Therefore, although advances have been made in intracellular labelling for EM, labelling is much easier and more established in fluorescence microscopy, which can achieve high molecular specificity for multiple targets. There is therefore a need for a high-resolution imaging methods that can image cell-material interactions live and in 3D, with easier sample preparation that enables the precise labelling of multiple specific intracellular and material components of interest **(Figure 2)**.

## Fluorescent Light Microscopy

Conventional fluorescent light microscopy (FLM) has been a fundamental technique for elucidating cell-material interactions. Specific sub-cellular targets can be labelled using antibodies, genetic probes and membrane binding dyes and multiple parameters can be labelled at once. Immunofluorescence (IF) uses fluorescently tagged antibodies or other molecules (such as phalloidin) which can interact

specifically with the protein of interest at high affinity. IF has been highly useful in characterizing the conformation, binding-availability and topography of adsorbed proteins on a material [91,92], as well as the response of cellular proteins involved in focal adhesion (FA) assembly and the resulting signaling pathways [6,15,93]. A downside of full-length antibodies is that they cannot be used to visualize intracellular events live, since they are relatively large on a nanoscale level and the cell needs to be permeabilized to allow them to access the cell interior. Antigen-binding fragments, such as single-domain antibodies and nanobodies show great promise in overcoming such obstacles but their preparation is time-consuming [94,95]. Alternatively, intracellular target proteins can be genetically labelled with proteins such as Green Fluorescent Protein (GFP) and can be non-invasively imaged live allowing dynamic interactions to be resolved *in-situ*. Genetic labelling must also be treated with caution however since it can impact the sample's properties. For example, the adhesive and signaling properties of integrin heterodimers have been shown to be dependent on whether the alpha- or beta-subunit of the heterodimer is labelled, since the integrin is partially activated when the beta-subunit is tagged [96].

A drawback of conventional FLM however is that its resolution is limited by the diffraction limit of light, as described by Ernst Abbé in 1873: $D = \lambda/2NA$, where D is the diffraction limit, $\lambda$ is the wavelength of the light, and NA is the numerical aperture. The wavelength of light and the numerical aperture of a conventional optical system results in a diffraction limit of 200-300 nm in the lateral direction, and 500-700 nm in the axial direction for conventional FLM. The resolution limit can be described by the point spread function (PSF), which describes how the fluorescence of a point-like object is spread, or diffracted, in an image, giving an intensity distribution. If two fluorophores are contained within the PSF in conventional FLM they cannot be distinguished, and objects that are smaller than the PSF are visualized the same size as the PSF. This significantly affects the study of interactions between cells and their substrates, which typically occur at the nanoscale.

## Super-resolution microscopy and intracellular cell-material interactions

In 2014, the Nobel Prize in Chemistry was jointly awarded to Eric Betzig, Stefan W. Hell and William E. Moerner for the development of super-resolved fluorescence microscopy (SRM), which breaks the diffraction limit of conventional FLM and enables imaging at the nanoscale [97]. A variety of methods exist, which achieve super-resolution either by spatially modulating the fluorescence emission using patterned illumination (e.g. stimulated emission depletion microscopy (STED) and structured illumination microscopy (SIM)) or by stochastically switching on and off individual molecules using photo-switchable probes (e.g. stochastic optical reconstruction microscopy (STORM)), or photoactivatable/photoconvertible fluorescent proteins (e.g. photoactivation localization microscopy (PALM)) [98]. It is crucial that the right SRM technique is chosen for a given sample and scientific question in hand.

Super-resolution microscopy has resolved a variety of intracellular, secreted and surface structures including ECM proteins [99], integrins [100–102], FAs [101,103], cytoskeletal components [104–110], nuclear pore complexes [111–115], the nuclear lamina [116], chromatin domains [117,118], lysosomes and vesicles [119,120], and many more organelles and sub-cellular structures [121] **(Figure 6)**. Indeed, structures such as integrins, FAs, and the cytoskeleton are critical for cells to sense their surroundings and it is important that they can be imaged dynamically and at high resolution to understand how cells interact with different materials. Moreover, the imaging of lysosomes and vesicles is useful in the assessment of cellular uptake and subsequent trafficking of nanomaterials.

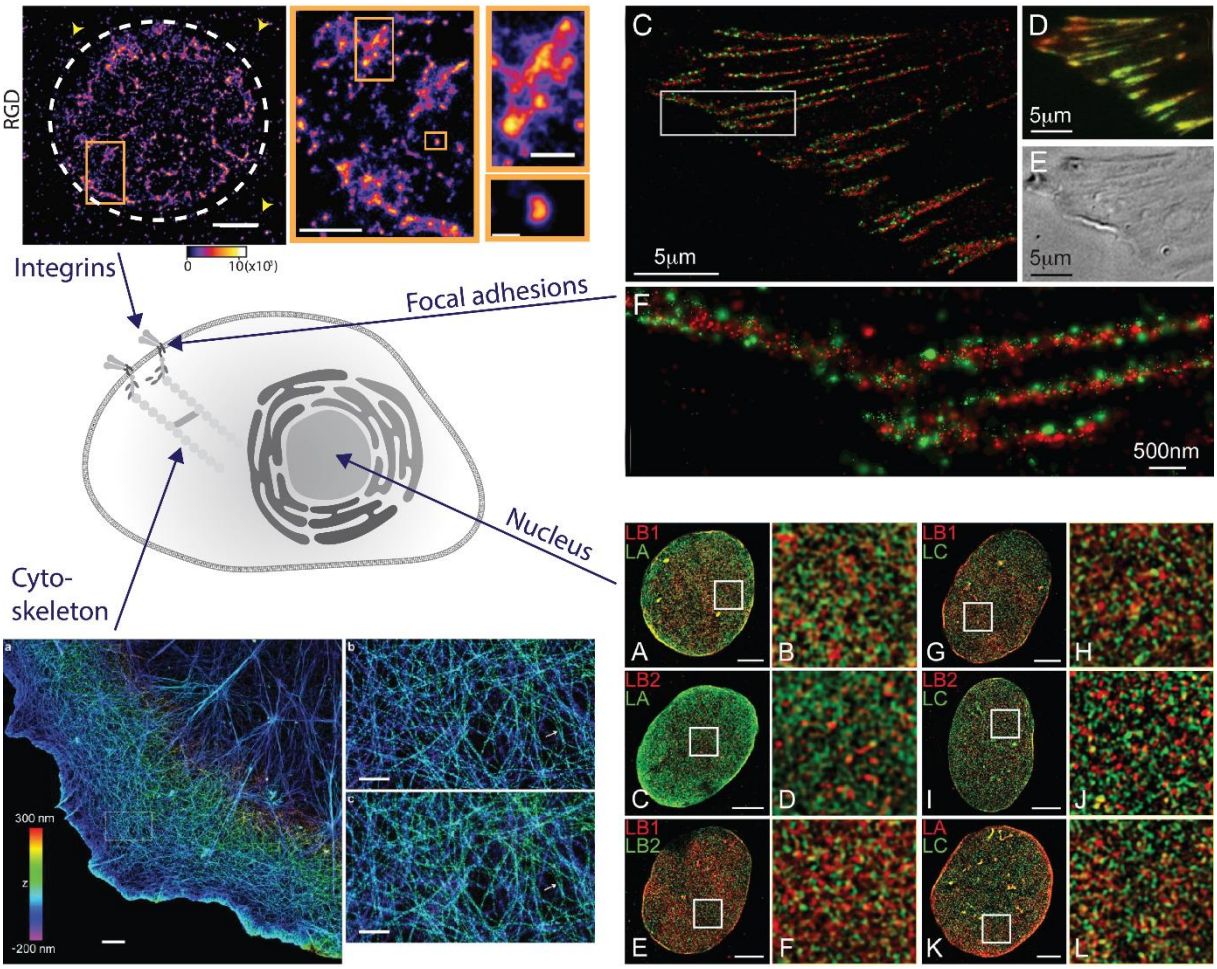


*Figure 6: Super-resolution microscopy (SRM) of intracellular organelles. SRM has been used to image intracellular organelles such as integrins, focal adhesions, the cytoskeleton and the nucleus at high resolution.* ***Integrins****: Photoactivation localization microscopy (PALM) image of integrins in a mouse embryonic fibroblast. Scale bar = 5 µm. 2 and 3: zoom of marked regions. Scale bars represent 2 µm (2), 500 nm (top), and 200 nm (bottom) (3). The false color scheme indicates density of molecules per square micrometer. Adapted from Changede et al., Developmental Cell, 35 (5), 614–621, 2015* [102]*, with permission from Elsevier, copyright 2015.* ***Focal adhesions****: (C&F) Dual-color PALM overlay of tdEos-tagged paxillin (green) and PS-CFP2-tagged zyxin (red) focal adhesion proteins. (D) Diffraction-limited, summed molecule, dual-color TIRF (total internal reflection fluorescent) microscope image. (E) Differential interference contrast (DIC) image. The two adhesion proteins seem co-localized in the TIRF microscope image but are shown to have very little overlap in the PALM images. Adapted from Shroff et al., Proceedings of the National Academy of Sciences, 104(51), 20308–20313, 2007,* [122] *with permission from the National Academy of Sciences, copyright 2007.* ***Nucleus****: 3D-structured illumination microscopy (SIM) imaging of lamin isoform in mouse embryonic fibroblasts. (A, B) lamin B1/ lamin A, (C, D) lamin B2/ lamin A, (E, F) lamin B1/ lamin B2, (G, H) lamin B1/ lamin C, (I, J) lamin B2/ lamin C, and (K, L) lamin A/ lamin C. B, D, F, H, J, and L, are 5x zoom-ins of the white boxed regions in A, C, E, G, I, and K respectively. Scale bar, 5 µm. Adapted from van der Shimi et al., Molecular Biology of the Cell, 26(22), 4075–4086, 2015* [116] *with permission from The American Society for Cell Biology, copyright 2015.* ***Cytoskeleton****: (a) Dual-objective stochastic optical reconstruction microscopy (STORM) image of the actin cytoskeleton in a COS-7 cell. The z positions are color coded with violet being the closest to the substrate and red being the farthest. (b) Zoom-in of the boxed region in (a). (c) Zoom-in of the boxed region in (a) using information only collected by objective one of the dual-objective setups. Scale bars, 2 µm (a), 500 nm (b–c). Adapted from Xu et al., Nature Methods, 9(2), 185–188, 2012* [110]*, with permission from Springer Nature, copyright 2012.*

Interestingly, the application of SRM to study cell-material interactions at the nanoscale is rather unexplored. This might be due to the small microscope working distance for SMLM techniques, and while other SRM techniques with slightly less resolution achieve slightly better z reconstructions, these can still be limiting for materials. Furthermore, it is also difficult to fluorescently label dense material structures, and this can prohibit an understanding of the material's nanotopography. However, the fluorescent labelling of surface chemistry structures would be highly useful in quantifying integrin-adhesion ligand bonds, for example. More recently, SRM has been used to investigate material properties [123,124] such as polymers [125,126], catalysts [127], DNA origami [128–130], lipid-based materials [131–133] and self-assembled materials [134]. SRM will be highly advantageous when looking at cell interactions with soft materials such as polymers since EM has issues with contrast in soft material due to the lack of heavy elements with significant electron numbers [135]. The key SRM techniques will now be described, as well as their advantages and disadvantages for the investigation of intracellular interactions with materials.

## Structured illumination microscopy (SIM) for simple sample preparation with moderate resolution improvement

Structured illumination microscopy is a wide-field technique that uses a patterned (usually striped) excitation beam that is fully rotated in steps between the capture of each image set **(Figure 3)**. The patterned excitation beam interacts with the sample to produce a Moiré effect that enables high frequency information to be obtained at lower spatial frequencies. Thus, usually non-resolvable structural information is captured. Following processing with a specialized algorithm, high-frequency sub-diffraction sample information can be extracted from the raw data to produce a reconstructed image with a two-fold improvement in lateral resolution (in comparison to conventional FLM techniques) and an axial resolution down to 150 nm [136]. Approaches such as instant SIM [137] and nonlinear SIM [138] have enabled spatial resolutions of 50 nm and temporal resolutions of 30 ms to be achieved.

Although SIM only has a moderate resolution improvement compared to other SRM techniques, a key advantage of SIM is that it is compatible with all conventional fluorophores and mounting conditions facilitating simpler sample preparation as well as 3- and 4-color imaging [139]. SIM has been used to demonstrate how cells interact with a number of biomaterials. For example, SIM has been used to visualize how the nucleus of primary human cells interacts with nanoneedle arrays. The nuclei were shown to remodel around the nanoneedles, which were fluorescently labelled to enable the tight interaction between the nuclei and nanoneedles to be demonstrated. Moreover, SIM revealed remodeling of lamin A/C but no remodeling of lamin B around the nanoneedles (**Figure 7a**) [140]. SIM has also been used to visualize the interactions between actin stress fibers, the nuclear lamina and LINC (Linker of Nucleoskeleton and Cytoskeleton) proteins in endothelial cells spread on a fibronectin-coated rectangular micropattern (**Figure 7b**). The micropattern was used to restrict cell spreading which increased apical actin tension, deformed the nuclear lamina and increased LINC protein density by two-fold at the sites of nuclear deformation [141]. Lamin A/C deformation was shown to localize with apical stress fibers. This result was demonstrated by quantifying the normalized intensity of lamin A/C and actin along specific lines oriented across the long nuclear axis of the cell; the most intense lamin A/C signals were found in the presence of apical actin filaments. Although the micropattern was not labelled, SIM could have provided an extra color channel to visualize the cell-micropattern interaction in more detail: the fibronectin could have been fluorescently labelled and its interaction with the cell's integrins and FAs (which are connected to the actin cytoskeleton and therefore indirectly connected to the nuclear lamina and LINC proteins) could have been assessed and quantified at nanoscale resolution. As well as looking at cell-substrate interactions, SIM has been used to assess the

internalization, subsequent intracellular localization, and possible degradation/deformation of a variety of nanoparticles [142–148]. SIM has been deemed the SRM method of choice when imaging dense, 3D networks of fine (and therefore weakly labelled) structures such as actin [149]. Indeed, this technique could be favorable for labelling and assessing the interaction between cells and fine electrospun materials.

Structured illumination microscopy shows high potential for visualizing dynamic cell-material interactions live in 3D [150–152]. SIM uses lower light intensities than the other SRM methods and can take faster recordings over cell-sized fields of view, making it superior for live-cell imaging [153]. For example, it has been used to record the dynamics of ECM ligand Arg-Gly-Asp (RGD) cluster growth and movement in relation to early FAs (**Figure 7c**) [102], and has tracked cell-uptake of metal-organic frameworks [144]. Moreover, two-photon instant SIM has enabled the imaging of cells in thick, semi-transparent biological specimens, such as cells in a 3D-collagen matrix, and the live imaging of tumor-like cell spheroids [154]. As with all forms of live FLM, SIM has an inherent trade-off between spatial resolution, temporal resolution and phototoxicity, and when imaging in 3D, this trade-off becomes magnified. Light sheet microscopy (LSM) addresses these limitations and has therefore been combined with SIM [108,155]. LSM projects and sweeps a thin sheet of light through a specimen, capturing an image in each plane to produce a 3D image. This process is high speed and eliminates out-of-focus background which therefore increases axial resolution as well as reducing phototoxicity and photobleaching [108,155].

A downside of SIM is that it is prone to many artefacts. These can result from imprecise calibration of the system, refractive index mismatch between the immersion oil and embedding medium, a poor signal to noise ratio, and bleaching properties of the sample (since a number of rotated images are required for each plane) [156,157]. SIMcheck is a plugin from the open-source image analysis platform ImageJ/Fiji which can check resolution and data quality of SIM images and enables users to identify and avoid common problems associated with 3D-SIM data [158]. Moreover, the fairSIM plugin enables image reconstruction of SIM images, providing users with an alternative to the commercial SIM software [159].

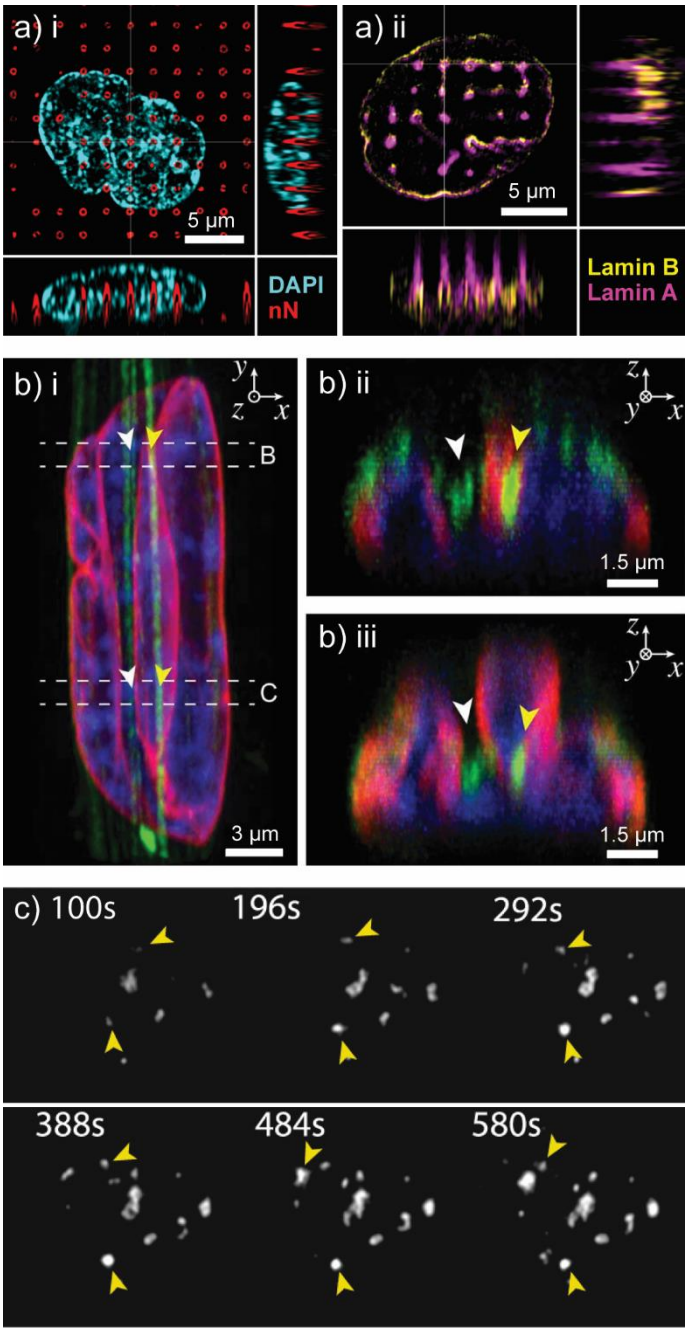


*Figure 7: Selected examples of structured illumination microscopy (SIM) applied to visualize cell-material interactions. a) 3D SIM orthogonal views of i) a nucleus interacting with a nanoneedle array with ii) remodeling of lamin A/C around the nanoneedles, but no remodeling of lamin B . Adapted from Hansel et al., ACS Nano, 2019* [140]*, with permission from the American Chemical Society, copyright 2019. b) 3D SIM orthogonal views to visualize the interactions between actin stress fibers and the nuclear envelope (DAPI and lamin AC) in cells spread on a fibronectin-coated rectangular micropattern that restricts cell spreading. Adapted from Versaevel, et al., Sci. Rep. 4, 7362, 2014* [141]*, with permission from Springer Nature, copyright 2014. c) Live SIM imaging to show the dynamics of ECM ligand Arg-Gly-Asp (RGD) cluster growth and movement in relation to early focal adhesions. Adapted from Changede et al., Dev. Cell 35, 614–621, 2015* [102]*, with permission from Elsevier, copyright 2015.*

## Stimulated emission depletion (STED) microscopy for high resolution 3D imaging with greater depth penetration

Stimulated emission depletion microscopy uses the same approach as a laser scanning confocal microscope but achieves higher resolution by reducing the size of the PSF by stimulated emission. In confocal laser-scanning microscopy, an objective lens is used to focus the excitation beam onto a small spot on the sample (the PSF) and this spot is scanned over the sample enabling a complete image to be obtained. All the fluorophores within this spot emit fluorescence and are detected and observed as a single pixel. The size of this PSF therefore limits the resolution of the image. In STED microscopy a STED laser is pulsed shortly after the normal excitation laser pulse. The STED beam overlaps with the excitation beam but has a doughnut shape with a hole at the center **(Figure 3)**. It has a longer wavelength than the excitation beam and produces photons that match the energy difference between the fluorophore's excited and ground states. The excited fluorophores are instantaneously 'bleached' back to the ground state by stimulated emission before spontaneous fluorescence emission can occur. Therefore, only the molecules in the center of the STED beam emit fluorescence, the PSF is reduced, and resolution can be increased to 20 nm in the lateral dimensions [160–163]. IsoSTED further increases the axial resolution through the coherent use of two opposing objective lenses (known as the 4Pi configuration), by means of a polarizing beam-splitter [164].

Stimulated emission depletion microscopy is advantageous compared to the other SRM techniques since super-resolution is achieved by optics alone and there is no need to computationally reconstruct images which evades image reconstruction artefacts. However, the laser power used for STED microscopy is considerably higher than many other SRM techniques, and could cause phototoxicity and photobleaching of samples. The high laser power may also be incompatible with some material systems, such as the imaging of cell interactions with gold nanoparticles: the high intensity STED laser could interact with gold nanoparticles to generate heat which could damage the sample [165,166]. Despite the high laser power ,which can cause phototoxicity and photobleaching, live-cell and *in vivo* STED microscopy has been conducted [167–169], and imaging modes such as dynamic intensity minimum (DyMIN) [170] and MINFIELD [171] have been developed which reduce the laser intensity and scanning sizes of the STED beam respectively. The high laser power can also affect choice of fluorophores for optimal output. Indeed the correct fluorophore and mounting conditions are key for a successful STED image, although conventional fluorophores and mounting conditions can be used [172]. STED has been used to image how nanoparticles such as nanodiamonds [173], carbon dots [174], protein-based fluorescent nanoparticles [175], and silica nanoparticles [176–178] are internalized within cells. For example, STED has shown that decorating nanodiamonds with albumin prevents their clustering inside cells [173] (**Figure 8a)** and has enabled the differentiation of membrane-bound and internalized silica nanoparticles [176] **(Figure 8b)**. Furthermore, STED has been used to quantify the average size of vinculin FAs on homogenous and nanopatterned fibronectin substrates of different sizes (**Figure 8c**). It was shown that the diameter of the FAs correlated with the diameter of the fibronectin nanopatterns [179].

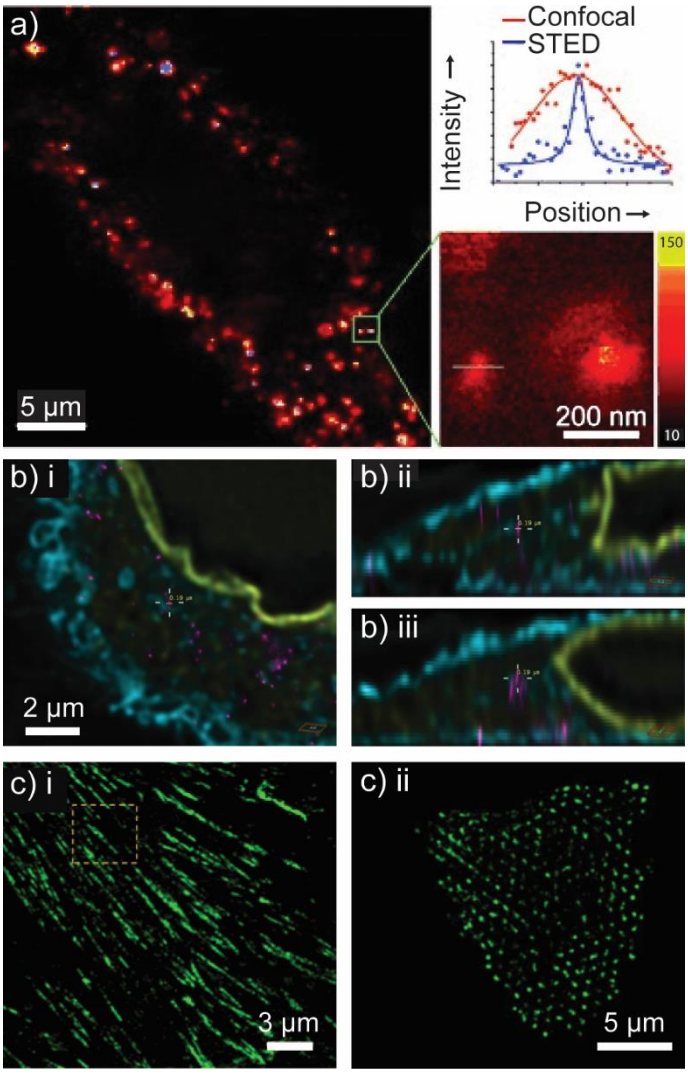


*Figure 8: Selected examples of stimulated emission depletion (STED) microscopy applied to visualize cell-material interactions. a) STED imaging of bovine serum albumin (BSA)-conjugated fluorescent nanodiamonds < 42 nm in size internalized in cells. Adapted from Tzeng et al., Chemie Int. Ed. 50, 2262–2265, 2011* [173]*, with permission from John Wiley and Sons, copyright 2011. b) 3D STED imaging to quantify the internalization of 25 nm and 85 nm silica nanoparticles. Multi-color orthogonal views i) = xy, ii) = xz, iii) = yz of the nanoparticles (magenta) in STED mode, the cell membrane (cyan) and nuclear membrane (yellow) are imaged in regular confocal mode. Adapted from Peuschel et al., Biomed Res. Int. 2015, 1–16, 2015* [176]*, open access article. c) STED imaging of vinculin focal adhesion proteins on a c i) homogeneous fibronectin surface and a c ii) nanopatterned fibronectin surface of 250 nm pattern size. Adapted from Chien et al., Small.,* 2906–2913, *2011,* [179]*, with permission from John Wiley and Sons, copyright 2011.*

Whilst 3D cultures will be fundamental in helping to elucidate cellular interactions with their natural microenvironment, the use of 3D cultures also presents new challenges. Many imaging techniques rely on light being transmitted through the sample and therefore have limited penetration depths. For example, confocal microscopy has a tissue penetration of around 100 µm due to the scattering of light and technicalities associated with the microscope set-up [180]. This makes tasks such as visualizing cells deep within a scaffold, hydrogel or *in vivo* tissue imaging difficult. Multiphoton microscopy (MPM) provides a solution for imaging thick 3D cell cultures or tissue since it has more than a two-fold improvement in penetration depth compared to conventional confocal microscopy [181]. MPM works by exciting a fluorophore with two or more photons at the same time. Longer wavelength light (roughly

2-fold) is used since photon energy is inversely proportional to wavelength. Since excitation can only occur at the point where the photons coincide, fluorophore excitation is restricted to the plane of focus. This means that the excitation light is not scattered by fluorophores above and below the plane of focus and phototoxicity and photobleaching are reduced. Since STED is conducted on a confocal microscope, its virtues can be combined with those of multiphoton microscopy, enabling high resolution imaging of thicker and highly scattering media [182,183]. For example, dendritic spines have been imaged in dense and highly scattering brain tissue using two-photon STED [184,185]. Combined STED and multiphoton microscopy could therefore be highly valuable when evaluating cell interactions deep within a highly scattering material.

## Single molecule localization microscopy (SMLM) for a simple optical set-up and high resolution single-particle tracking

In conventional FLM most fluorophores emit fluorescence simultaneously within the PSF, and are therefore indistinguishable. SMLM techniques ensure that only a small, random subpopulation of fluorophores are switched on and recorded at any given time. That way neighboring fluorescent emitters do not overlap and each fluorophore can be isolated, identified and located at sub-diffraction precision **(Figure 3)**. This process of activation and inactivation is repeated over a high number of frames (few thousand to tens of thousands) to ensure all the molecules have been imaged and the resulting images are merged into a final image by post-processing. The resolution of this image mainly depends on the number of photons collected and a resolution of 20-30 nm can generally be achieved, going down to the 5 nm range with further optimization [110,186,187].

Single molecule localization microscopy has the advantage of a relatively simple wide-field optic setup and is often performed in total internal reflection fluorescent (TIRF) mode to reduce background. TIRF microscopy can image fluorophores close to the glass/water (or glass/specimen) interface at an axial resolution below 100 nm [188]. An evanescent wave is employed to excite the fluorophores; this occurs when the excitation beam is totally reflected at the interface of two transparent media with different refractive indices (e.g. the glass of the coverslip and the contact area of adhering cells). The energy of the evanescent field decreases exponentially with distance from the interface. As a result, only the fluorophores in close proximity to the interface are excited, and the background fluorescence from the fluorophores in the rest of the cell is removed. The disadvantage of TIRF microscopy is that only molecules in close proximity to the interface can be investigated. Therefore, wide-field setups are also employed for SMLM, although they have the disadvantage of a higher background.

STORM, PALM and fPALM, which were originally published in 2006, are examples of such stochastic imaging [120,189,190]. STORM originally involved photo-switchable dyes (cy3 and cy5) and two lasers: one low-power activating laser stochastically turns a small, random number of fluorophores on and then another high-power laser immediately turns all the fluorophores off. More often direct STORM (dSTORM) is used which exploits the intrinsic blinking properties of specific fluorophores. This blinking is coupled to the use of specific imaging buffers that scavenge molecular oxygen, pushing the fluorophore into a triplet ‘off’ state. Regulation of the number of fluorophores in the triplet state dictates the sparsity of detections [191]. The PALM techniques use a similar principle to STORM but employ photo-switchable protein tagged fluorophores (e.g. tandem dimer Eos and photoactivatable GFP, PA-GFP) instead of photo-switchable dyes [192]. PALM and STORM thus require fluorescent proteins or specific organic dyes which can stochastically blink under specific excitation schemes and buffer conditions. These fluorophores must also label their target structures with high labelling densities in order to fulfil the Nyquist-Shannon theorem, which requires the structure to be sampled at twice the rate of the intended resolution. Choice of dye, excitation conditions, buffer conditions and labelling density are therefore paramount in SMLM and must be heavily optimized [193–195]. Points accumulation for imaging in nanoscale topography (PAINT) is a SMLM method which overcomes the

constraints imposed by fluorophores. Here, the stochastic binding of a fluorescent ligand is exploited, rather than the stochastic photo-activation of a fluorophore [195,196]. Specific buffers and high laser powers are therefore not required as the blinking is not dependent on the fluorophore's photophysical properties. SMLM can image live cells in 3D with high spatial and temporal resolution [197], and six-color STORM images have been obtained [198].

Single molecule localization microscopy techniques have been used to visualize molecular reorganizations at the nanoscale when cells are interfaced with different materials (**Figure 9**). For example, dSTORM has been used to assess how homogeneous and nanopatterned fibronectin surfaces can affect FA formation [179]. dSTORM enabled the location of individual vinculin FA molecules to be located with an accuracy of around 20 nm and the spatial correlation between each vinculin protein was analyzed as well as the number and density of vinculin proteins in each FA. Moreover, PALM has been used to characterize and quantify early integrin clusters on RGD matrices of different stiffnesses at ∼10 nm resolution (**Figure 9a**) [102]. It was shown that very early adhesions consist of ∼100-nm clusters of ∼50 β3-activated integrins. These early adhesions formed similarly on flexible and rigid substrates, however most adhesions were transient on rigid substrates. In addition, combined PALM and highly inclined and laminated optical sheet (HILO) microscopy has been used to image the dynamics and molecular organization of cellular nanostructures on micropatterened substrates with a precision of 7-20 nm [199]. It was shown that caveolin-1 at the cell membrane, and emerin at the nuclear membrane undergo dynamic nanoscale structural organizations in response to steady-state mechanical cues induced by the micropatterns (**Figure 9b**).

To enable the rational design of safe and effective nanomedicines, the intracellular fate of nanoparticles must be understood [200,201]. Indeed, high-resolution multi-color imaging techniques that can image and quantify intracellular nanoparticles and how they are internalised (preferentially live and in 3D) will provide a means to understand the complex and numerous mechanisms involved in nanoparticle uptake [201]. In addition, it is also important to understand how nanoparticle parameters such as size, shape, and surface properties (chemistry and charge) impact the endocytic process [201]. SMLM techniques have the capacity to quantify cell-nanoparticle interactions directly at the single molecule level since each single molecule is localized and stored in an output file as a coordinate, and they have been used to track nanoparticle uptake and trafficking [202–205]. For example, processes such as nanoparticle engulfment and storage of nanoparticles in vesicles have been visualized at single-nanoparticle and single-endo/phago/lysosome resolution (**Figure 9c**) [202,203]. Moreover, the size distribution and chemistries (highlighted by different colored fluorophores) of intracellular nanoparticles has been accurately quantified [203]. Furthermore, PALM imaging has demonstrated that polystyrene particles can be uptaken by two distinct clathrin-mediated endocytosis pathways: for the majority of cases the nanoparticles initially attached to the membrane followed by the formation of a clathrin-coated pit, however events in which the nanoparticle diffused on the membrane and utilized a pre-formed clathrin-coated pit were also observed [204].

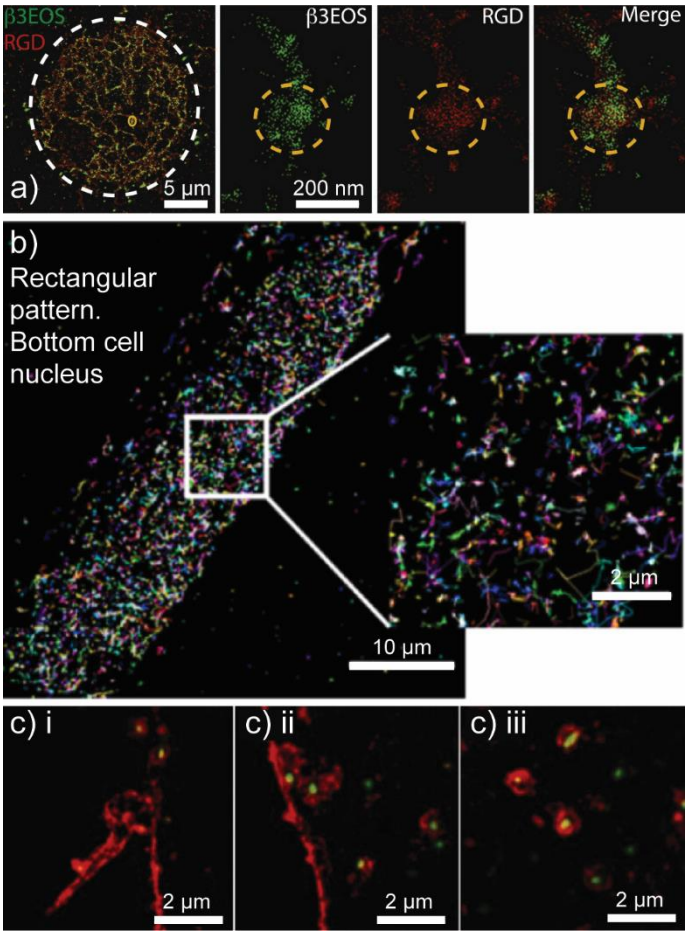


*Figure 9: Selected examples of single molecule localization microscopy (SMLM) applied to visualize cell-material interactions. a) Photo-activated localization microscopy (PALM) imaging of the relationship between integrins and RGD ligand clusters on functionalized fluid supported lipid bilayers. Adapted from Changede et al., Dev. Cell 35, 614–621, 2015* [102]*, with permission from Elsevier, copyright 2015. b) PALM single particle tracking to evaluate the diffusion trajectories of the nuclear protein emerin at the basal nuclear membrane of a deformed nucleus in a cell seeded on a 210 × 10 μm$^2$ micropattern. Adapted from Fernandez et al., ACS Appl. Mater. Interfaces, 9, 27575-27586, 2017* [199]*, with permission from the American Chemical Society, copyright 2017. c) STORM imaging of the internalization process of polymer hydrogel nanoparticles (green) by dendritic cells (cell membrane in red). i) cell membrane engulfment of the nanoparticles ii) intracellular routing and iii) storage of the nanoparticles in endo/lysosomal vesicles. Adapted from De Koker et al., Angew. Chemie - Int. Ed., 55, 1334-1339, 2015* [202]*, with permission from John Wiley and Sons, copyright 2015.*

## Fluorescence resonance energy transfer (FRET) for the quantification of high resolution interactions

Fluorescence resonance energy transfer (FRET) describes a mechanism that can be used to measure nanoscale distances between two chromophores using FLM. A donor chromophore in its excited electronic state transfers energy to an acceptor chromophore *via* nonradiative dipole-dipole coupling. By measuring FRET efficiency, the distance between two chromophores can be determined at nanoscale resolution (up to 2-8 nm) since FRET is inversely proportional to the sixth power of the distance between the donor and acceptor chromophore [206].

There are few methods to directly quantify cell-material interactions at the molecular level, and the cellular response is often correlated to the general properties of the material (e.g. elasticity). However, this is not an accurate assessment of cell-material interactions since the cell is also responding to other stimuli, such as soluble stimuli, and the cell-material interface is not static. FRET has been used to quantitatively assess specific parameters of the cell-material interface in both 2D and 3D. For example, molecular changes in matrix proteins, the number of bonds between integrins and their ligands, and changes in the cross-linking density of hydrogels have been recorded using FRET [207]. Indeed FRET could be highly useful for the quantitative assessment of how cellular signaling pathways respond to a material interfaces dynamically in 3D.

# Future outlooks

## Light sheet microscopy (LSM) for live 3D imaging

Living cells are highly sensitive to perturbations in their surroundings and it is therefore of high importance that they are imaged in their native environments under gentle illumination conditions. LSM is an ideal technique for live 3D imaging with minimal sample perturbation since a single optical section of the sample is illuminated at a time, with no illumination above or below the section, minimizing phototoxic events [208]. In addition, since an entire optical slice can be collected in one go, it can be detected by a camera, which enables sub-second volumetric imaging. LSM would therefore be the microscopy technique of choice for monitoring rapid dynamic intracellular responses to biomaterials over prolonged periods; however, it is not a super-resolution technique. Fortunately, LSM can be combined with super-resolution techniques such as SIM, STED, and SMLM [209]. Lattice LSM (LLSM), which combines LSM with Bessel beam microscopy and SIM, has recently been combined with adaptive optics (AO), which correct refractive index aberrations, to study a variety of subcellular events within whole transparent organisms [210]. Intracellular dynamics, extracellular communication and collective cell behaviors could therefore potentially be studied in thick transparent scaffolds and hydrogels using AO-LLSM. Moreover, delivery of nanoparticles could also be monitored in whole transparent organisms such as zebrafish. Combined LSM and SRM imaging could thus further our understanding of dynamic nanoscale interactions between cells and biomaterials.

## Correlative light and electron microscopy (CLEM): combining the advantages of electron microscopy and super-resolution microscopy

Super-resolution microscopy is advantageous compared to EM for cell-material interactions since it can image specific intracellular components and how they respond to materials both live and in 3D. It is clear that each SRM technique has its own key advantages: SIM is most appealing for live, multicolor imaging; STED has advantages for deep 3D imaging; and SMLM is advantageous when wanting to quantify and localise events on a simple microscope. However, SRM techniques also exhibit certain limitations: SIM only provides a 2-fold increase in resolution compared to conventional FLM and is prone to artefacts; STED has high laser powers which can cause photobleaching and damage the cell and substrate; SMLM techniques are highly reliant on fluorophore selection and imaging conditions. Although SRM techniques can localize labelled structures at very high accuracy, they do not provide information about the position of the labels in relation to the cell ultrastructure and it is hard to label dense materials. There are clear advantages and disadvantages for both SRM and EM when imaging intracellular interactions with biomaterials (**Table 1**). These limitations can be overcome through the use of correlative light and electron microscopy (CLEM) [211]. The imaging of a sample with both microscopy techniques produces results that maximize the strengths of each technique while minimizing their individual weaknesses.

Super-resolution microscopy and EM have successfully been correlated to image the same sample [120], however the main challenge lies in the sample preparation [212,213]. To begin with, sample preparation protocols for the different techniques may be incompatible. Critical EM sample preparation steps such as chemical fixation, heavy-metal staining and resin embedding quench fluorescence, may alter a fluorophore's photo-switching ability, and can also lead to stronger background autofluorescence [211]. This is detrimental for SRM since it requires a high signal-to-noise ratio. A number of sample preparation workflows have therefore been developed to enable super-resolution CLEM. For example, a photoactivatable fluorescent protein has been developed which does not lose its fluorescence after the heavy $OsO_4$ fixation required for EM imaging [214]. Moreover, cryo-fixed resin embedded samples have been produced which preserve the fluorescence and photo-switching ability of fluorescent proteins [215], and graphene has been shown to act as an ultrathin barrier material enabling CLEM of hydrated cells [216]. Super-resolution cryo-CLEM is a promising technique that could provide super-resolution imaging of samples with structural preservation in the native state [217], however it comes with a variety of technical challenges that need to be addressed [218].

Correlative light and electron microscopy allows the direct and live examination of fluorescently labelled molecules within the high-resolution landscape of EM images. Live light microscopy has been performed in correlation with EM [219], and since SRM imaging has been conducted on live samples it is therefore feasible that live SRM imaging could be combined with EM, correlating cell ultrastructure to dynamics and function. CLEM could enable the advantages of both EM and SRM techniques to be combined for the imaging of cell-material interactions.

*Table 1: Comparison of electron microscopy (EM) and super-resolution microscopy (SRM) for cell-material interactions*

| | EM | SRM |
|---|---|---|
| Advantages | • Near atomic resolution [49]<br>• Can image the cell ultrastructure<br>• Can image the surface nanotopography of materials without the need of labelling<br>• Continuous 3D cross-sectioning *in situ* with immunogold labelling (focused ion beam scanning electron microscopy, FIB-SEM) [62] | • Live 3D imaging [151,168,197]<br>• Multicolor imaging [139,220,221]<br>• Conventional fluorophores and mounting conditions (structured illumination microscopy, SIM and stimulated emission depletion microscopy, STED)<br>• Simple optic set-up (single molecule localization microscopy, SMLM)<br>• Single-particle tracking (SMLM) for nanoparticle internalization experiments [203] |
| Disadvantages | • Single section therefore 2D, with potential artefacts on sectioning (TEM) [65]<br>• Complex and time-consuming sample set up<br>• Availability of equipment (FIB-SEM)<br>• Live imaging may be impossible to attain [74] | • Complex data processing (SIM and SMLM) with possible artefacts from image reconstruction<br>• Cannot image cell ultrastructure<br>• Cannot image a material's nanotopography without fluorescent labelling (unless it is autofluorescent in a different channel to the label)<br>• High labelling density required (STED and SMLM) [149]<br>• High photobleaching (particularly for STED) [222] |

| | | |
|---|---|---|
| | | • Specialized probes and optimization of mounting conditions required (SMLM) [193] |

## Conclusion

Physical and chemical cues presented on the surface of materials can affect cell function and fate. Indeed, biomaterials with various nanoscale topographies, stiffnesses and surface functionalities have been shown to trigger intracellular signaling pathways, and nanoparticles show great promise for the delivery of biomolecules into cells. It is of high importance that these interactions are better understood for the improved design of cell manipulation/delivery strategies. The visualization of specific organelles and nanomaterials and quantification of their morphology and interactions at high spatial and temporal resolution within the context of the cell ultrastructure will be key in understanding such cell-material interactions. An ideal imaging system for cell-material interactions would image in 3D at significant depths with facile sample preparation and minimal artefacts. Multi-color SRM imaging enables multiple cellular components to be resolved simultaneously and unambiguously both live and in 3D at nanoscale resolution whilst EM provides cellular ultrastructure and material topography at nanoscale resolution. A combination of both SRM and EM (CLEM) will therefore be critical for the visualization of cell-material interactions at the nanoscale.

## Acknowledgements

C.S.H. acknowledges support from the Engineering and Physical Sciences Research Council (EPSRC, EP/F500416/1). M.N.H. acknowledges support from the FP7 Marie Curie Intra-European Fellowship "SMase LIPOSOME" [626766] and the National Research Programme "Smart Materials" of the Swiss National Science Foundation [P300PA_171540 and 406240_147493]. S.G. was funded by a PhD studentship in Biomedicine and Bioengineering in Osteoarthritis, Imperial College London. M.M.S. acknowledges support from a Wellcome Trust Senior Investigator Award [098411/Z/12/Z], the grant from the UK Regenerative Medicine Platform “Acellular / Smart Materials – 3D Architecture” [MR/R015651/1], the ERC Seventh Framework Programme Consolidator grant “Naturale CG” [616417], the Swedish Foundation of Strategic Research through the Industrial Research Centre “FoRmulaEx” [IRC15-0065] and the Research Council of Norway through its Centres of Excellence scheme (262613). The authors would like to thank A. Nogiwa-Valdez for administrative support, and S. A. Maynard and Q. Chen for carefully reading through the review and providing suggestions.

## Author contributions

C.S.H. prepared the manuscript; M.H. made the figures and contributed to the electron microscopy section; S.G. contributed to the electron microscopy sections; M.M.S. designed the manuscript scope and revised the manuscript.

## Conflict of interest

The authors declare no conflict of interest.

# References


[1] V. Vogel, Unraveling the mechanobiology of extracellular matrix, Annu. Rev. Physiol. 80 (2018) 353–387. doi:10.1146/annurev-physiol-021317-121312.

[2] A.P. Liu, O. Chaudhuri, S.H. Parekh, New advances in probing cell-extracellular matrix interactions, Integr. Biol. (United Kingdom). 9 (2017) 383–405. doi:10.1039/c6ib00251j.

[3] M.M. Stevens, J.H. George, Exploring and engineering the cell surface interface, Science (80-. ). 310 (2005) 1135–1138. doi:10.1126/science.1106587.

[4] S.W. Crowder, V. Leonardo, T. Whittaker, P. Papathanasiou, M.M. Stevens, Material cues as potent regulators of epigenetics and stem cell function, Cell Stem Cell. 18 (2016) 39–52. doi:10.1016/j.stem.2015.12.012.

[5] R.J. McMurray, N. Gadegaard, P.M. Tsimbouri, K. V. Burgess, L.E. McNamara, R. Tare, K. Murawski, E. Kingham, R.O.C. Oreffo, M.J. Dalby, Nanoscale surfaces for the long-term maintenance of mesenchymal stem cell phenotype and multipotency, Nat. Mater. 10 (2011) 637–644. doi:10.1038/nmat3058.

[6] W. Chen, L.G. Villa-Diaz, Y. Sun, S. Weng, J.K. Kim, R.H.W. Lam, L. Han, R. Fan, P.H. Krebsbach, J. Fu, Nanotopography influences adhesion, spreading, and self-renewal of human embryonic stem cells, ACS Nano. 6 (2012) 4094–4103. doi:10.1021/nn3004923.

[7] Y.P. Kong, C.H. Tu, P.J. Donovan, A.F. Yee, Expression of Oct4 in human embryonic stem cells is dependent on nanotopographical configuration, Acta Biomater. 9 (2013) 6369–6380. doi:10.1016/j.actbio.2013.01.036.

[8] M.J. Dalby, M.O. Riehle, H.J.H. Johnstone, S. Affrossman, A.S.G. Curtis, Polymer-demixed nanotopography: Control of fibroblast spreading and proliferation, Tissue Eng. 8 (2003) 1099–1108. doi:10.1089/107632702320934191.

[9] A.S.G. Curtis, B. Casey, J.O. Gallagher, D. Pasqui, M.A. Wood, C.D.W. Wilkinson, Substratum nanotopography and the adhesion of biological cells. Are symmetry or regularity of nanotopography important?, Biophys. Chem. 94 (2001) 275–283. doi:10.1016/S0301-4622(01)00247-2.

[10] J.O. Gallagher, K.F. McGhee, C.D.W. Wilkinson, M.O. Riehle, Interaction of animal cells with ordered nanotopography, IEEE Trans. Nanobioscience. 1 (2002) 24–28. doi:10.1109/TNB.2002.806918.

[11] M.J. Dalby, N. Gadegaard, R. Tare, A. Andar, M.O. Riehle, P. Herzyk, C.D.W. Wilkinson, R.O.C. Oreffo, The control of human mesenchymal cell differentiation using nanoscale symmetry and disorder, Nat. Mater. 6 (2007) 997–1003. doi:10.1038/nmat2013.

[12] A.J. Engler, S. Sen, H.L. Sweeney, D.E. Discher, Matrix elasticity directs stem cell lineage specification., Cell. 126 (2006) 677–89. doi:10.1016/j.cell.2006.06.044.

[13] H.J. Kong, J. Liu, K. Riddle, T. Matsumoto, K. Leach, D.J. Mooney, Non-viral gene delivery regulated by stiffness of cell adhesion substrates, Nat. Mater. 4 (2005) 460–464. doi:10.1038/nmat1392.

[14] M. Guvendiren, J.A. Burdick, Stiffening hydrogels to probe short- and long-term cellular responses to dynamic mechanics, Nat. Commun. 3 (2012) 792. doi:10.1038/ncomms1792.

[15] J. Swift, I.L. Ivanovska, A. Buxboim, T. Harada, P.C.D.P. Dingal, J. Pinter, J.D. Pajerowski, K.R. Spinler, J.W. Shin, M. Tewari, F. Rehfeldt, D.W. Speicher, D.E. Discher, Nuclear lamin-A scales with tissue stiffness and enhances matrix-directed differentiation, Science (80-. ). 341 (2013) 1240104–1240104. doi:10.1126/science.1240104.

[16] R. McBeath, D.M. Pirone, C.M. Nelson, K. Bhadriraju, C.S. Chen, Cell shape, cytoskeletal tension, and RhoA regulate stem cell lineage commitment., Dev. Cell. 6 (2004) 483–95. doi:10.1016/S1534-5807(04)00075-9.

[17] G. Abagnale, A. Sechi, M. Steger, Q. Zhou, C.C. Kuo, G. Aydin, C. Schalla, G. Müller-Newen, M. Zenke, I.G. Costa, P. van Rijn, A. Gillner, W. Wagner, Surface topography guides morphology and spatial patterning of induced pluripotent stem cell colonies, Stem Cell Reports. 9 (2017)

654–666. doi:10.1016/j.stemcr.2017.06.016.
[18] J.B. Recknor, D.S. Sakaguchi, S.K. Mallapragada, Directed growth and selective differentiation of neural progenitor cells on micropatterned polymer substrates, Biomaterials. 27 (2006) 4098–4108. doi:10.1016/j.biomaterials.2006.03.029.
[19] N. Gomez, S. Chen, C.E. Schmidt, Polarization of hippocampal neurons with competitive surface stimuli: Contact guidance cues are preferred over chemical ligands, J. R. Soc. Interface. 4 (2007) 223–233. doi:10.1098/rsif.2006.0171.
[20] M.R. Lee, K.W. Kwon, H. Jung, H.N. Kim, K.Y. Suh, K. Kim, K.S. Kim, Direct differentiation of human embryonic stem cells into selective neurons on nanoscale ridge/groove pattern arrays, Biomaterials. 31 (2010) 4360–4366. doi:10.1016/j.biomaterials.2010.02.012.
[21] C. Morez, M. Noseda, M.A. Paiva, E. Belian, M.D. Schneider, M.M. Stevens, Enhanced efficiency of genetic programming toward cardiomyocyte creation through topographical cues, Biomaterials. 70 (2015) 94–104. doi:10.1016/j.biomaterials.2015.07.063.
[22] T.L. Downing, J. Soto, C. Morez, T. Houssin, A. Fritz, F. Yuan, J. Chu, S. Patel, D. V. Schaffer, S. Li, Biophysical regulation of epigenetic state and cell reprogramming, Nat. Mater. 12 (2013) 1154–1162. doi:10.1038/nmat3777.
[23] J. Sia, P. Yu, D. Srivastava, S. Li, Effect of biophysical cues on reprogramming to cardiomyocytes, Biomaterials. 103 (2016) 1–11. doi:10.1016/j.biomaterials.2016.06.034.
[24] T.C. von Erlach, S. Bertazzo, M.A. Wozniak, C.-M. Horejs, S.A. Maynard, S. Attwood, B.K. Robinson, H. Autefage, C. Kallepitis, A. Del Río Hernández, C.S. Chen, S. Goldoni, M.M. Stevens, Cell-geometry-dependent changes in plasma membrane order direct stem cell signalling and fate., Nat. Mater. 17 (2018) 237–242. doi:10.1038/s41563-017-0014-0.
[25] J.M. Curran, R. Chen, J.A. Hunt, Controlling the phenotype and function of mesenchymal stem cells in vitro by adhesion to silane-modified clean glass surfaces, Biomaterials. 26 (2005) 7057–7067. doi:10.1016/j.biomaterials.2005.05.008.
[26] J.M. Curran, R. Chen, J.A. Hunt, The guidance of human mesenchymal stem cell differentiation in vitro by controlled modifications to the cell substrate, Biomaterials. 27 (2006) 4783–4793. doi:10.1016/j.biomaterials.2006.05.001.
[27] D.S.W. Benoit, M.P. Schwartz, A.R. Durney, K.S. Anseth, Small functional groups for controlled differentiation of hydrogel-encapsulated human mesenchymal stem cells, Nat. Mater. 7 (2008) 816–823. doi:10.1038/nmat2269.
[28] C.M. Horejs, J.P. St-Pierre, J.R.M. Ojala, J.A.M. Steele, P.B. Da Silva, A. Rynne-Vidal, S.A. Maynard, C.S. Hansel, C. Rodríguez-Fernández, M.M. Mazo, A.Y.F. You, A.J. Wang, T. Von Erlach, K. Tryggvason, M. López-Cabrera, M.M. Stevens, Preventing tissue fibrosis by local biomaterials interfacing of specific cryptic extracellular matrix information, Nat. Commun. 8 (2017) 15509. doi:10.1038/ncomms15509.
[29] C.-M. Horejs, A. Serio, A. Purvis, A.J. Gormley, S. Bertazzo, A. Poliniewicz, A.J. Wang, P. DiMaggio, E. Hohenester, M.M. Stevens, Biologically-active laminin-111 fragment that modulates the epithelial-to-mesenchymal transition in embryonic stem cells, Proc. Natl. Acad. Sci. 111 (2014) 5908–5913. doi:10.1073/pnas.1403139111.
[30] V. Llopis-Hernández, M. Cantini, C. González-García, Z.A. Cheng, J. Yang, P.M. Tsimbouri, A.J. García, M.J. Dalby, M. Salmerón-Sánchez, Material-driven fibronectin assembly for high-efficiency presentation of growth factors, Sci. Adv. 2 (2016) e1600188. doi:10.1126/sciadv.1600188.
[31] B.L. Beckstead, D.M. Santosa, C.M. Giachelli, Mimicking cell-cell interactions at the biomaterial-cell interface for control of stem cell differentiation, J. Biomed. Mater. Res. - Part A. 79 (2006) 94–103. doi:10.1002/jbm.a.30760.
[32] L. Li, J.R. Klim, R. Derda, A.H. Courtney, L.L. Kiessling, Spatial control of cell fate using synthetic surfaces to potentiate TGF- signaling, Proc. Natl. Acad. Sci. 108 (2011) 11745–11750. doi:10.1073/pnas.1101454108.
[33] V. Mailänder, K. Landfester, Interaction of nanoparticles with cells, Biomacromolecules. 10 (2009) 2379–2400. doi:10.1021/bm900266r.

[34] A. Verma, F. Stellacci, Effect of surface properties on nanoparticle-cell interactions, Small. 6 (2010) 12–21. doi:10.1002/smll.200901158.
[35] J.B. Delehanty, H. Mattoussi, I.L. Medintz, Delivering quantum dots into cells: Strategies, progress and remaining issues, Anal. Bioanal. Chem. 393 (2009) 1091–1105. doi:10.1007/s00216-008-2410-4.
[36] S.A.A. Rizvi, A.M. Saleh, Applications of nanoparticle systems in drug delivery technology, Saudi Pharm. J. 26 (2018) 64–70. doi:10.1016/j.jsps.2017.10.012.
[37] S. Gopal, C. Chiappini, J. Penders, V. Leonardo, H. Seong, S. Rothery, Y. Korchev, A. Shevchuk, M.M. Stevens, Porous silicon nanoneedles modulate endocytosis to deliver biological payloads, Adv. Mater. 31 (2019) 1806788. doi:10.1002/adma.201806788.
[38] C. Chiappini, J.O. Martinez, E. De Rosa, C.S. Almeida, E. Tasciotti, M.M. Stevens, Biodegradable nanoneedles for localized delivery of nanoparticles in vivo: Exploring the biointerface, ACS Nano. 9 (2015) 5500–5509. doi:10.1021/acsnano.5b01490.
[39] C. Chiappini, E. De Rosa, J.O. Martinez, X. Liu, J. Steele, M.M. Stevens, E. Tasciotti, Biodegradable silicon nanoneedles delivering nucleic acids intracellularly induce localized in vivo neovascularization, Nat. Mater. 14 (2015) 532–539. doi:10.1038/nmat4249.
[40] F. Variola, Atomic force microscopy in biomaterials surface science, Phys. Chem. Chem. Phys. 17 (2015) 2950–2959. doi:10.1039/C4CP04427D.
[41] A. Shevchuk, S. Tokar, S. Gopal, J.L. Sanchez-Alonso, A.I. Tarasov, A.C. Vélez-Ortega, C. Chiappini, P. Rorsman, M.M. Stevens, J. Gorelik, G.I. Frolenkov, D. Klenerman, Y.E. Korchev, Angular approach ccanning ion conductance microscopy, Biophys. J. 110 (2016) 2252–2265. doi:10.1016/J.BPJ.2016.04.017.
[42] W. Hällström, T. Mårtensson, C. Prinz, P. Gustavsson, L. Montelius, L. Samuelson, M. Kanje, Gallium phosphide nanowires as a substrate for cultured neurons, Nano Lett. 7 (2007) 2960–2965. doi:10.1021/nl070728e.
[43] J. Schindelin, I. Arganda-Carreras, E. Frise, V. Kaynig, M. Longair, T. Pietzsch, S. Preibisch, C. Rueden, S. Saalfeld, B. Schmid, J.-Y. Tinevez, D.J. White, V. Hartenstein, K. Eliceiri, P. Tomancak, A. Cardona, Fiji: an open-source platform for biological-image analysis, Nat. Methods. 9 (2012) 676–682. doi:10.1038/nmeth.2019.
[44] M.D. Abramoff, P.J. Magalhães, S.J. Ram, Image Processing with ImageJ, Biophotonics Int. 11 (2004) 36–42. https://dspace.library.uu.nl/handle/1874/204900.
[45] A.E. Carpenter, T.R. Jones, M.R. Lamprecht, C. Clarke, I. Kang, O. Friman, D.A. Guertin, J. Chang, R.A. Lindquist, J. Moffat, P. Golland, D.M. Sabatini, CellProfiler: image analysis software for identifying and quantifying cell phenotypes, Genome Biol. 7 (2006) R100. doi:10.1186/gb-2006-7-10-r100.
[46] F. De Chaumont, S. Dallongeville, J.C. Olivo-Marin, ICY: A new open-source community image processing software, in: Proc. - Int. Symp. Biomed. Imaging, IEEE, 2011: pp. 234–237. doi:10.1109/ISBI.2011.5872395.
[47] H. Peng, F. Long, Seeing more is knowing more: V3D enables real-time 3D visualization and quantitative analysis of large-scale biological image data sets, Lect. Notes Comput. Sci. (Including Subser. Lect. Notes Artif. Intell. Lect. Notes Bioinformatics). 6577 LNBI (2011) 336. doi:10.1007/978-3-642-20036-6_30.
[48] J.C. Caicedo, S. Cooper, F. Heigwer, S. Warchal, P. Qiu, C. Molnar, A.S. Vasilevich, J.D. Barry, H.S. Bansal, O. Kraus, M. Wawer, L. Paavolainen, M.D. Herrmann, M. Rohban, J. Hung, H. Hennig, J. Concannon, I. Smith, P.A. Clemons, S. Singh, P. Rees, P. Horvath, R.G. Linington, A.E. Carpenter, Data-analysis strategies for image-based cell profiling, Nat. Methods. 14 (2017) 849–863. doi:10.1038/nmeth.4397.
[49] K. Murata, M. Wolf, Cryo-electron microscopy for structural analysis of dynamic biological macromolecules, Biochim. Biophys. Acta - Gen. Subj. 1862 (2018) 324–334. doi:10.1016/j.bbagen.2017.07.020.
[50] A. Leal-Egaña, U. Dietrich-Braumann, A. Díaz-Cuenca, M. Nowicki, A. Bader, Determination of pore size distribution at the cell-hydrogel interface, J. Nanobiotechnology. 9 (2011) 24.

doi:10.1186/1477-3155-9-24.
[51] E.Y.X. Loh, N. Mohamad, M.B. Fauzi, M.H. Ng, S.F. Ng, M.C.I. Mohd Amin, Development of a bacterial cellulose-based hydrogel cell carrier containing keratinocytes and fibroblasts for full-thickness wound healing, Sci. Rep. 8 (2018) 2875. doi:10.1038/s41598-018-21174-7.
[52] B. Baharloo, M. Textor, D.M. Brunette, Substratum roughness alters the growth, area, and focal adhesions of epithelial cells, and their proximity to titanium surfaces, J. Biomed. Mater. Res. - Part A. 74 (2005) 12–22. doi:10.1002/jbm.a.30321.
[53] G. Wrobel, M. Höller, S. Ingebrandt, S. Dieluweit, F. Sommerhage, H.P. Bochem, A. Offenhäusser, Transmission electron microscopy study of the cell-sensor interface, J. R. Soc. Interface. 5 (2008) 213–222. doi:10.1098/rsif.2007.1094.
[54] L. Hanson, Z.C. Lin, C. Xie, Y. Cui, B. Cui, Characterization of the cell-nanopillar interface by transmission electron microscopy, Nano Lett. 12 (2012) 5815–5820. doi:10.1021/nl303163y.
[55] A. Fendyur, N. Mazurski, J. Shappir, M.E. Spira, Formation of essential ultrastructural interface between cultured hippocampal cells and gold mushroom-shaped MEA- toward “IN-CELL” recordings from vertebrate neurons, Front. Neuroeng. 4 (2011) 14. doi:10.3389/fneng.2011.00014.
[56] R.F. Egerton, Electron energy-loss spectroscopy in the TEM, Reports Prog. Phys. 72 (2009) 016502. doi:10.1088/0034-4885/72/1/016502.
[57] M.A. Aronova, R.D. Leapman, Development of electron energy-loss spectroscopy in the biological sciences, MRS Bull. 37 (2012) 53–62. doi:10.1557/mrs.2011.329.
[58] X. Wang, F.A. Shah, A. Palmquist, K. Grandfield, 3D characterization of human nano-osseointegration by on-axis electron tomography without the missing wedge, ACS Biomater. Sci. Eng. 3 (2017) 49–55. doi:10.1021/acsbiomaterials.6b00519.
[59] G.E. Palade, A study of fixation for electron microscopy, J. Exp. Med. 95 (1952) 285–298. doi:10.1084/jem.95.3.285.
[60] J.G. Hirsch, M.E. Fedorko, Ultrastructure of human leukocytes after simultaneous fixation with glutaraldehyde and osmium tetroxide and “postfixation” in uranyl acetate., J. Cell Biol. 38 (1968) 615–627. doi:10.1083/jcb.38.3.615.
[61] T.M. Mayhew, C. Mühlfeld, D. Vanhecke, M. Ochs, A review of recent methods for efficiently quantifying immunogold and other nanoparticles using TEM sections through cells, tissues and organs, Ann. Anat. 191 (2009) 153–170. doi:10.1016/j.aanat.2008.11.001.
[62] S. Gopal, C. Chiappini, J.P.K. Armstrong, Q. Chen, A. Serio, C.-C. Hsu, C. Meinert, T.J. Klein, D.W. Hutmacher, S. Rothery, M.M. Stevens, Immunogold FIB-SEM: Combining volumetric ultrastructure visualization with 3D biomolecular analysis to dissect cell-environment interactions, Adv. Mater. (2019) 1900488. doi:10.1002/adma.201900488.
[63] J. Dubochet, M. Adrian, J.J. Chang, J.C. Homo, J. Lepault, A.W. McDowall, P. Schultz, Cryo-electron microscopy of vitrified specimens., Q. Rev. Biophys. 21 (1988) 129–228. http://www.ncbi.nlm.nih.gov/pubmed/3043536 (accessed July 8, 2019).
[64] V. Lučić, A. Rigort, W. Baumeister, Cryo-electron tomography: The challenge of doing structural biology in situ, J. Cell Biol. 202 (2013) 407–419. doi:10.1083/jcb.201304193.
[65] H.K. Edwards, M.W. Fay, S.I. Anderson, C.A. Scotchford, D.M. Grant, P.D. Brown, An appraisal of ultramicrotomy, FIBSEM and cryogenic FIBSEM techniques for the sectioning of biological cells on titanium substrates for TEM investigation, J. Microsc. 234 (2009) 16–25. doi:10.1111/j.1365-2818.2009.03152.x.
[66] L.A. Giannuzzi, F.A. Stevie, A review of focused ion beam milling techniques for TEM specimen preparation, Micron. 30 (1999) 197–204. doi:10.1016/S0968-4328(99)00005-0.
[67] S. Elsharkawy, M. Al-Jawad, M.F. Pantano, E. Tejeda-Montes, K. Mehta, H. Jamal, S. Agarwal, K. Shuturminska, A. Rice, N. V. Tarakina, R.M. Wilson, A.J. Bushby, M. Alonso, J.C. Rodriguez-Cabello, E. Barbieri, A. Del Río Hernández, M.M. Stevens, N.M. Pugno, P. Anderson, A. Mata, Protein disorder-order interplay to guide the growth of hierarchical mineralized structures, Nat. Commun. 9 (2018) 2145. doi:10.1038/s41467-018-04319-0.
[68] A. Hoenger, J.R. McIntosh, Probing the macromolecular organization of cells by electron

tomography, Curr. Opin. Cell Biol. 21 (2009) 89–96. doi:10.1016/j.ceb.2008.12.003.
[69] F.K.M. Schur, M. Obr, W.J.H. Hagen, W. Wan, A.J. Jakobi, J.M. Kirkpatrick, C. Sachse, H.G. Kräusslich, J.A.G. Briggs, An atomic model of HIV-1 capsid-SP1 reveals structures regulating assembly and maturation, Science (80-. ). 353 (2016) 506–508. doi:10.1126/science.aaf9620.
[70] M.F. Hohmann-Marriott, A.A. Sousa, A.A. Azari, S. Glushakova, G. Zhang, J. Zimmerberg, R.D. Leapman, Nanoscale 3D cellular imaging by axial scanning transmission electron tomography, Nat. Methods. 6 (2009) 729–731. doi:10.1038/nmeth.1367.
[71] M. Elbaum, S.G. Wolf, L. Houben, Cryo-scanning transmission electron tomography of biological cells, MRS Bull. 41 (2016) 542–548. doi:10.1557/mrs.2016.136.
[72] C. Zhu, S. Liang, E. Song, Y. Zhou, W. Wang, F. Shan, Y. Shi, C. Hao, K. Yin, T. Zhang, J. Liu, H. Zheng, L. Sun, In-situ liquid cell transmission electron microscopy investigation on oriented attachment of gold nanoparticles, Nat. Commun. 9 (2018) 421. doi:10.1038/s41467-018-02925-6.
[73] Y. Zhang, D. Keller, M.D. Rossell, R. Erni, Formation of Au nanoparticles in liquid cell transmission electron microscopy: From a systematic study to engineered nanostructures, 2017. doi:10.1021/acs.chemmater.7b04421.
[74] N. De Jonge, D.B. Peckys, Live cell electron microscopy is probably impossible, ACS Nano. 10 (2016) 9061–9063. doi:10.1021/acsnano.6b02809.
[75] C.J. Peddie, L.M. Collinson, Exploring the third dimension: Volume electron microscopy comes of age, Micron. 61 (2014) 9–19. doi:10.1016/j.micron.2014.01.009.
[76] F. Santoro, W. Zhao, L.M. Joubert, L. Duan, J. Schnitker, Y. Van De Burgt, H.Y. Lou, B. Liu, A. Salleo, L. Cui, Y. Cui, B. Cui, Revealing the cell-material interface with nanometer resolution by Focused Ion Beam/Scanning Electron Microscopy, ACS Nano. 11 (2017) 8320–8328. doi:10.1021/acsnano.7b03494.
[77] M. Dipalo, A.F. McGuire, H.Y. Lou, V. Caprettini, G. Melle, G. Bruno, C. Lubrano, L. Matino, X. Li, F. De Angelis, B. Cui, F. Santoro, Cells adhering to 3D vertical nanostructures: Cell membrane reshaping without stable internalization, Nano Lett. 18 (2018) 6100–6105. doi:10.1021/acs.nanolett.8b03163.
[78] R. Wierzbicki, C. Købler, M.R.B. Jensen, J. Łopacińska, M.S. Schmidt, M. Skolimowski, F. Abeille, K. Qvortrup, K. Mølhave, Mapping the complex morphology of cell interactions with nanowire substrates using FIB-SEM, PLoS One. 8 (2013) e53307. doi:10.1371/journal.pone.0053307.
[79] H. Persson, C. Købler, K. Mølhave, L. Samuelson, J.O. Tegenfeldt, S. Oredsson, C.N. Prinz, Fibroblasts cultured on nanowires exhibit low motility, impaired cell division, and DNA damage, Small. 9 (2013) 4006–4016. doi:10.1002/smll.201300644.
[80] J.J. Li, A. Akey, C.R. Dunstan, M. Vielreicher, O. Friedrich, D.C. Bell, H. Zreiqat, Effects of material–tissue interactions on bone regeneration outcomes using baghdadite implants in a large animal model, Adv. Healthc. Mater. 7 (2018) 1800218. doi:10.1002/adhm.201800218.
[81] M. Olderøy, M.B. Lilledahl, M.S. Beckwith, J.E. Melvik, F. Reinholt, P. Sikorski, J.E. Brinchmann, Biochemical and structural characterization of neocartilage formed by mesenchymal stem cells in alginate hydrogels, PLoS One. 9 (2014) e91662. doi:10.1371/journal.pone.0091662.
[82] A.J. Koster, J. Klumperman, Electron microscopy in cell biology: Integrating structure and function., Nat. Rev. Mol. Cell Biol. Suppl (2003) SS6-10. doi:10.1038/nrm1194.
[83] R.C.N. Melo, E. Morgan, R. Monahan-Earley, A.M. Dvorak, P.F. Weller, Pre-embedding immunogold labeling to optimize protein localization at subcellular compartments and membrane microdomains of leukocytes, Nat. Protoc. 9 (2014) 2382–2394. doi:10.1038/nprot.2014.163.
[84] E. Evergren, N. Tomilin, E. Vasylieva, V. Sergeeva, O. Bloom, H. Gad, F. Capani, O. Shupliakov, A pre-embedding immunogold approach for detection of synaptic endocytic proteins in situ, J. Neurosci. Methods. 135 (2004) 169–174. doi:10.1016/j.jneumeth.2003.12.010.
[85] B.M. Humbel, M.D.M. De Jong, W.H. Müller, A.J. Verkleij, Pre-embedding immunolabeling for electron microscopy: An evaluation of permeabilization methods and markers, Microsc. Res.

Tech. 42 (1998) 43–58. doi:10.1002/(SICI)1097-0029(19980701)42:1<43::AID-JEMT6>3.0.CO;2-S.
[86] H. Yi, J.L.M. Leunissen, G.M. Shi, C.A. Gutekunst, S.M. Hersch, A novel procedure for pre-embedding double immunogold-silver labeling at the ultrastructural level, J. Histochem. Cytochem. 49 (2001) 279–283. doi:10.1177/002215540104900301.
[87] M.H. Ellisman, T.J. Deerinck, X. Shu, G.E. Sosinsky, Picking faces out of a crowd: Genetic labels for identification of proteins in correlated light and electron microscopy imaging, in: Methods Cell Biol., 2012: pp. 139–155. doi:10.1016/B978-0-12-416026-2.00008-X.
[88] J.D. Martell, T.J. Deerinck, S.S. Lam, M.H. Ellisman, A.Y. Ting, Electron microscopy using the genetically encoded APEX2 tag in cultured mammalian cells, Nat. Protoc. 12 (2017) 1792–1816. doi:10.1038/nprot.2017.065.
[89] J.D. Martell, T.J. Deerinck, Y. Sancak, T.L. Poulos, V.K. Mootha, G.E. Sosinsky, M.H. Ellisman, A.Y. Ting, Engineered ascorbate peroxidase as a genetically encoded reporter for electron microscopy, Nat. Biotechnol. 30 (2012) 1143–1148. doi:10.1038/nbt.2375.
[90] C. Hopkins, A. Gibson, J. Stinchcombe, C. Futter, Chimeric molecules employing horseradish peroxidase as reporter enzyme for protein localization in the electron microscope, Methods Enzymol. 327 (2000) 35–45. doi:10.1016/S0076-6879(00)27265-0.
[91] C.J. Wilson, R.E. Clegg, D.I. Leavesley, M.J. Pearcy, Mediation of biomaterial–cell interactions by adsorbed proteins: A review, Tissue Eng. 11 (2005) 1–18. doi:10.1089/ten.2005.11.1.
[92] F. Grinnell, M.K. Feld, Fibronectin adsorption on hydrophilic and hydrophobic surfaces detected by antibody binding and analyzed during cell adhesion in serum-containing medium., J. Biol. Chem. 257 (1982) 4888–4893. doi:7068668.
[93] S. Dupont, L. Morsut, M. Aragona, E. Enzo, S. Giulitti, M. Cordenonsi, F. Zanconato, J. Le Digabel, M. Forcato, S. Bicciato, N. Elvassore, S. Piccolo, Role of YAP/TAZ in mechanotransduction., Nature. 474 (2011) 179–83. doi:10.1038/nature10137.
[94] B. Traenkle, U. Rothbauer, Under the microscope: Single-domain antibodies for live-cell imaging and super-resolution microscopy, Front. Immunol. 8 (2017) 1030. doi:10.3389/fimmu.2017.01030.
[95] E. Beghein, J. Gettemans, Nanobody technology: A versatile toolkit for microscopic imaging, protein-protein interaction analysis, and protein function exploration, Front. Immunol. 8 (2017) 771. doi:10.3389/fimmu.2017.00771.
[96] C.G. Galbraith, M.W. Davidson, J.A. Galbraith, A cautionary tail: Changes in integrin behavior with labeling, BioRxiv. (2017) 158618. doi:10.1101/158618.
[97] L. Möckl, D.C. Lamb, C. Bräuchle, Super-resolved fluorescence microscopy: Nobel Prize in Chemistry 2014 for Eric Betzig, Stefan Hell, and William E. Moerner, Angew. Chemie Int. Ed. 53 (2014) 13972–13977. doi:10.1002/anie.201410265.
[98] L. Schermelleh, A. Ferrand, T. Huser, C. Eggeling, M. Sauer, O. Biehlmaier, G.P.C. Drummen, Super-resolution microscopy demystified, Nat. Cell Biol. 21 (2019) 72–84. doi:10.1038/s41556-018-0251-8.
[99] S.M. Früh, I. Schoen, J. Ries, V. Vogel, Molecular architecture of native fibronectin fibrils, Nat. Commun. 6 (2015) 7275. doi:10.1038/ncomms8275.
[100] T.I. Moore, J. Aaron, T.L. Chew, T.A. Springer, Measuring integrin conformational change on the cell surface with super-resolution microscopy, Cell Rep. 22 (2018) 1903–1912. doi:10.1016/j.celrep.2018.01.062.
[101] P. Kanchanawong, G. Shtengel, A.M. Pasapera, E.B. Ramko, M.W. Davidson, H.F. Hess, C.M. Waterman, Nanoscale architecture of integrin-based cell adhesions., Nature. 468 (2010) 580–4. doi:10.1038/nature09621.
[102] R. Changede, X. Xu, F. Margadant, M.P. Sheetz, Nascent integrin adhesions form on all matrix rigidities after integrin activation, Dev. Cell. 35 (2015) 614–621. doi:10.1016/j.devcel.2015.11.001.
[103] H. Deschout, T. Lukes, A. Sharipov, D. Szlag, L. Feletti, W. Vandenberg, P. Dedecker, J. Hofkens, M. Leutenegger, T. Lasser, A. Radenovic, Complementarity of PALM and SOFI for super-

resolution live-cell imaging of focal adhesions, Nat. Commun. 7 (2016) 13693. doi:10.1038/ncomms13693.
[104] S. Bretschneider, C. Eggeling, S.W. Hell, Breaking the diffraction barrier in fluorescence microscopy by optical shelving, Phys. Rev. Lett. 98 (2007) 218103. doi:10.1103/PhysRevLett.98.218103.
[105] S.A. Finkenstaedt-Quinn, T.A. Qiu, K. Shin, C.L. Haynes, Super-resolution imaging for monitoring cytoskeleton dynamics, Analyst. 141 (2016) 5674–5688. doi:10.1039/c6an00731g.
[106] L. Pan, R. Yan, W. Li, K. Xu, Super-resolution microscopy reveals the native ultrastructure of the erythrocyte cytoskeleton, Cell Rep. 22 (2018) 1151–1158. doi:10.1016/j.celrep.2017.12.107.
[107] H.Y. Suleiman, R. Roth, S. Jain, J.E. Heuser, A.S. Shaw, J.H. Miner, Injury-induced actin cytoskeleton reorganization in podocytes revealed by super-resolution microscopy, JCI Insight. 2 (2017). doi:10.1172/jci.insight.94137.
[108] D. Li, L. Shao, B.-C. Chen, X. Zhang, M. Zhang, B. Moses, D.E. Milkie, J.R. Beach, J.A. Hammer, M. Pasham, T. Kirchhausen, M.A. Baird, M.W. Davidson, P. Xu, E. Betzig, Extended-resolution structured illumination imaging of endocytic and cytoskeletal dynamics, Science (80-. ). 349 (2015) aab3500–aab3500. doi:10.1126/science.aab3500.
[109] Z. Zhang, Y. Nishimura, P. Kanchanawong, Extracting microtubule networks from superresolution single-molecule localization microscopy data, Mol. Biol. Cell. 28 (2017) 333–345. doi:10.1091/mbc.e16-06-0421.
[110] K. Xu, H.P. Babcock, X. Zhuang, Dual-objective STORM reveals three-dimensional filament organization in the actin cytoskeleton, Nat. Methods. 9 (2012) 185–188. doi:10.1038/nmeth.1841.
[111] A. Loschberger, S. van de Linde, M.-C. Dabauvalle, B. Rieger, M. Heilemann, G. Krohne, M. Sauer, Super-resolution imaging visualizes the eightfold symmetry of gp210 proteins around the nuclear pore complex and resolves the central channel with nanometer resolution, J. Cell Sci. 125 (2012) 570–575. doi:10.1242/jcs.098822.
[112] J. Ma, J.M. Kelich, S.L. Junod, W. Yang, Super-resolution mapping of scaffold nucleoporins in the nuclear pore complex, J. Cell Sci. 130 (2017) 1299–1306. doi:10.1242/jcs.193912.
[113] J. Sellés, M. Penrad-Mobayed, C. Guillaume, A. Fuger, L. Auvray, O. Faklaris, F. Montel, Nuclear pore complex plasticity during developmental process as revealed by super-resolution microscopy, Sci. Rep. 7 (2017) 14732. doi:10.1038/s41598-017-15433-2.
[114] A. Szymborska, A. De Marco, N. Daigle, V.C. Cordes, J.A.G. Briggs, J. Ellenberg, Nuclear pore scaffold structure analyzed by super-resolution microscopy and particle averaging, Science (80-. ). 341 (2013) 655–658. doi:10.1126/science.1240672.
[115] W. Xie, A. Chojnowski, T. Boudier, J.S.Y. Lim, S. Ahmed, Z. Ser, C. Stewart, B. Burke, A-type lamins form distinct filamentous networks with differential nuclear pore complex associations, Curr. Biol. 26 (2016) 2651–2658. doi:10.1016/j.cub.2016.07.049.
[116] T. Shimi, M. Kittisopikul, J. Tran, A.E. Goldman, S.A. Adam, Y. Zheng, K. Jaqaman, R.D. Goldman, Structural organization of nuclear lamins A, C, B1, and B2 revealed by superresolution microscopy, Mol. Biol. Cell. 26 (2015) 4075–4086. doi:10.1091/mbc.E15-07-0461.
[117] B.J. Beliveau, A.N. Boettiger, M.S. Avendaño, R. Jungmann, R.B. McCole, E.F. Joyce, C. Kim-Kiselak, F. Bantignies, C.Y. Fonseka, J. Erceg, M.A. Hannan, H.G. Hoang, D. Colognori, J.T. Lee, W.M. Shih, P. Yin, X. Zhuang, C.T. Wu, Single-molecule super-resolution imaging of chromosomes and in situ haplotype visualization using Oligopaint FISH probes, Nat. Commun. 6 (2015) 7147. doi:10.1038/ncomms8147.
[118] A.N. Boettiger, B. Bintu, J.R. Moffitt, S. Wang, B.J. Beliveau, G. Fudenberg, M. Imakaev, L.A. Mirny, C. Wu, X. Zhuang, Super-resolution imaging reveals distinct chromatin folding for different epigenetic states., Nature. 529 (2016) 418–22. doi:10.1038/nature16496.
[119] V. Westphal, S.O. Rizzoli, M.A. Lauterbach, D. Kamin, R. Jahn, S.W. Hell, Video-rate far-field optical nanoscopy dissects synaptic vesicle movement, Science (80-. ). 320 (2008) 246–249.

doi:10.1126/science.1154228.
[120] E. Betzig, G.H. Patterson, R. Sougrat, O.W. Lindwasser, S. Olenych, J.S. Bonifacino, M.W. Davidson, J. Lippincott-Schwartz, H.F. Hess, Imaging intracellular fluorescent proteins at nanometer resolution, Science (80-. ). 313 (2006) 1642–1645. doi:10.1126/science.1127344.
[121] S.J. Sahl, S.W. Hell, S. Jakobs, Fluorescence nanoscopy in cell biology, Nat. Rev. Mol. Cell Biol. 18 (2017) 685–701. doi:10.1038/nrm.2017.71.
[122] H. Shroff, C.G. Galbraith, J.A. Galbraith, H. White, J. Gillette, S. Olenych, M.W. Davidson, E. Betzig, Dual-color superresolution imaging of genetically expressed probes within individual adhesion complexes, Proc. Natl. Acad. Sci. 104 (2007) 20308–20313. doi:10.1073/pnas.0710517105.
[123] D. Wöll, C. Flors, Super-resolution fluorescence imaging for materials science, Small Methods. 1 (2017) 1700191. doi:10.1002/smtd.201700191.
[124] S. Pujals, N. Feiner-Gracia, P. Delcanale, I. Voets, L. Albertazzi, Super-resolution microscopy as a powerful tool to study complex synthetic materials, Nat. Rev. Chem. 3 (2019) 68–84. doi:10.1038/s41570-018-0070-2.
[125] H. Park, D.T. Hoang, K. Paeng, L.J. Kaufman, Localizing exciton recombination sites in conformationally distinct single conjugated polymers by super-resolution fluorescence imaging, ACS Nano. 9 (2015) 3151–3158. doi:10.1021/acsnano.5b00086.
[126] B.E. Urban, B. Dong, T.Q. Nguyen, V. Backman, C. Sun, H.F. Zhang, Subsurface super-resolution imaging of unstained polymer nanostructures, Sci. Rep. 6 (2016) 28156. doi:10.1038/srep28156.
[127] K.P.F. Janssen, G. De Cremer, R.K. Neely, A. V. Kubarev, J. Van Loon, J.A. Martens, D.E. De Vos, M.B.J. Roeffaers, J. Hofkens, Single molecule methods for the study of catalysis: From enzymes to heterogeneous catalysts, Chem. Soc. Rev. 43 (2014) 990–1006. doi:10.1039/c3cs60245a.
[128] R. Iinuma, Y. Ke, R. Jungmann, T. Schlichthaerle, J.B. Woehrstein, P. Yin, Polyhedra self-assembled from DNA tripods and characterized with 3D DNA-PAINT, Science (80-. ). 344 (2014) 65–69. doi:10.1126/science.1250944.
[129] C. Steinhauer, R. Jungmann, T.L. Sobey, F.C. Simmel, P. Tinnefeld, DNA origami as a nanoscopic ruler for superresolution microscopy, Angew. Chemie - Int. Ed. 48 (2009) 8870–8873. doi:10.1002/anie.200903308.
[130] J.J. Schmied, C. Forthmann, E. Pibiri, B. Lalkens, P. Nickels, T. Liedl, P. Tinnefeld, DNA origami nanopillars as standards for three-dimensional superresolution microscopy, Nano Lett. 13 (2013) 781–785. doi:10.1021/nl304492y.
[131] A. Sharonov, R.M. Hochstrasser, Wide-field subdiffraction imaging by accumulated binding of diffusing probes, Proc. Natl. Acad. Sci. 103 (2006) 18911–18916. doi:10.1073/pnas.0609643104.
[132] A. Boreham, P. Volz, D. Peters, C.M. Keck, U. Alexiev, Determination of nanostructures and drug distribution in lipid nanoparticles by single molecule microscopy, Eur. J. Pharm. Biopharm. 110 (2017) 31–38. doi:10.1016/j.ejpb.2016.10.020.
[133] L. Belfiore, L.M. Spenkelink, M. Ranson, A.M. van Oijen, K.L. Vine, Quantification of ligand density and stoichiometry on the surface of liposomes using single-molecule fluorescence imaging, J. Control. Release. 278 (2018) 80–86. doi:10.1016/j.jconrel.2018.03.022.
[134] L. Albertazzi, D. Van Der Zwaag, C.M.A. Leenders, R. Fitzner, R.W. Van Der Hofstad, E.W. Meijer, Probing exchange pathways in one-dimensional aggregates with super-resolution microscopy, Science (80-. ). 344 (2014) 491–495. doi:10.1126/science.1250945.
[135] K. Friedemann, A. Turshatov, K. Landfester, D. Crespy, Characterization via two-color STED microscopy of nanostructured materials synthesized by colloid electrospinning, Langmuir. 27 (2011) 7132–7139. doi:10.1021/la104817r.
[136] M.G.L. Gustafsson, Surpassing the lateral resolution limit by a factor of two using structured illumination microscopy, J. Microsc. 198 (2000) 82–87. doi:10.1046/j.1365-2818.2000.00710.x.

[137] A.G. York, P. Chandris, D.D. Nogare, J. Head, P. Wawrzusin, R.S. Fischer, A. Chitnis, H. Shroff, Instant super-resolution imaging in live cells and embryos via analog image processing, Nat. Methods. 10 (2013) 1122–1130. doi:10.1038/nmeth.2687.
[138] M.G.L. Gustafsson, Nonlinear structured-illumination microscopy: Wide-field fluorescence imaging with theoretically unlimited resolution, Proc. Natl. Acad. Sci. 102 (2005) 13081–13086. doi:10.1073/pnas.0406877102.
[139] L. Schermelleh, P.M. Carlton, S. Haase, L. Shao, L. Winoto, P. Kner, B. Burke, M.C. Cardoso, D.A. Agard, M.G.L. Gustafsson, H. Leonhardt, J.W. Sedat, Subdiffraction multicolor imaging of the nuclear periphery with 3D structured illumination microscopy, Science (80-. ). 320 (2008) 1332–1336. doi:10.1126/science.1156947.
[140] C.S. Hansel, S.W. Crowder, S. Cooper, S. Gopal, M. Joaio Pardelha Da Cruz, L. De Oliveira Martins, D. Keller, S. Rothery, M. Becce, A.E.G. Cass, C. Bakal, C. Chiappini, M.M. Stevens, Nanoneedle-mediated stimulation of cell mechanotransduction machinery, ACS Nano. 13 (2019) 2913–2926. doi:10.1021/acsnano.8b06998.
[141] M. Versaevel, J.B. Braquenier, M. Riaz, T. Grevesse, J. Lantoine, S. Gabriele, Super-resolution microscopy reveals LINC complex recruitment at nuclear indentation sites, Sci. Rep. 4 (2014) 7362. doi:10.1038/srep07362.
[142] X. Chen, J. Cui, H. Sun, M. Müllner, Y. Yan, K.F. Noi, Y. Ping, F. Caruso, Analysing intracellular deformation of polymer capsules using structured illumination microscopy, Nanoscale. 8 (2016) 11924–11931. doi:10.1039/c6nr02151d.
[143] F. Cavalieri, G.L. Beretta, J. Cui, J.A. Braunger, Y. Yan, J.J. Richardson, S. Tinelli, M. Folini, N. Zaffaroni, F. Caruso, Redox-sensitive PEG-polypeptide nanoporous particles for survivin silencing in prostate cancer cells, Biomacromolecules. 16 (2015) 2168–2178. doi:10.1021/acs.biomac.5b00562.
[144] M.H. Teplensky, M. Fantham, P. Li, T.C. Wang, J.P. Mehta, L.J. Young, P.Z. Moghadam, J.T. Hupp, O.K. Farha, C.F. Kaminski, D. Fairen-Jimenez, Temperature treatment of highly porous zirconium-containing metal-organic frameworks extends drug delivery release, J. Am. Chem. Soc. 139 (2017) 7522–7532. doi:10.1021/jacs.7b01451.
[145] E. Tolstik, L.A. Osminkina, C. Matthäus, M. Burkhardt, K.E. Tsurikov, U.A. Natashina, V.Y. Timoshenko, R. Heintzmann, J. Popp, V. Sivakov, Studies of silicon nanoparticles uptake and biodegradation in cancer cells by Raman spectroscopy, Nanomedicine Nanotechnology, Biol. Med. 12 (2016) 1931–1940. doi:10.1016/j.nano.2016.04.004.
[146] E. Tolstik, L.A. Osminkina, D. Akimov, M.B. Gongalsky, A.A. Kudryavtsev, V.Y. Timoshenko, R. Heintzmann, V. Sivakov, J. Popp, Linear and non-linear optical imaging of cancer cells with silicon nanoparticles, Int. J. Mol. Sci. 17 (2016) 1536. doi:10.3390/ijms17091536.
[147] J. Cui, B. Hibbs, S.T. Gunawan, J.A. Braunger, X. Chen, J.J. Richardson, E. Hanssen, F. Caruso, Immobilized particle imaging for quantification of nano- and microparticles, Langmuir. 32 (2016) 3532–3540. doi:10.1021/acs.langmuir.6b00229.
[148] X. Chen, J. Cui, Y. Ping, T. Suma, F. Cavalieri, Q.A. Besford, G. Chen, J.A. Braunger, F. Caruso, Probing cell internalisation mechanics with polymer capsules, Nanoscale. 8 (2016) 17096–17101. doi:10.1039/c6nr06657g.
[149] E. Wegel, A. Göhler, B.C. Lagerholm, A. Wainman, S. Uphoff, R. Kaufmann, I.M. Dobbie, Imaging cellular structures in super-resolution with SIM, STED and Localisation Microscopy: A practical comparison, Sci. Rep. 6 (2016) 27290. doi:10.1038/srep27290.
[150] R. Fiolka, L. Shao, E.H. Rego, M.W. Davidson, M.G.L. Gustafsson, Time-lapse two-color 3D imaging of live cells with doubled resolution using structured illumination., Proc. Natl. Acad. Sci. U. S. A. 109 (2012) 5311–5. doi:10.1073/pnas.1119262109.
[151] L. Shao, P. Kner, E.H. Rego, M.G.L. Gustafsson, Super-resolution 3D microscopy of live whole cells using structured illumination, Nat. Methods. 8 (2011) 1044–1048. doi:10.1038/nmeth.1734.
[152] A.G. Godin, B. Lounis, L. Cognet, Super-resolution microscopy approaches for live cell imaging, Biophys. J. 107 (2014) 1777–1784. doi:10.1016/j.bpj.2014.08.028.

[153] P. Kner, B.B. Chhun, E.R. Griffis, L. Winoto, M.G.L. Gustafsson, Super-resolution video microscopy of live cells by structured illumination, Nat. Methods. 6 (2009) 339–342. doi:10.1038/nmeth.1324.
[154] P.W. Winter, P. Chandris, R.S. Fischer, Y. Wu, C.M. Waterman, H. Shroff, Incoherent structured illumination improves optical sectioning and contrast in multiphoton super-resolution microscopy., Opt. Express. 23 (2015) 5327–34. doi:10.1364/OE.23.005327.
[155] B.C. Chen, W.R. Legant, K. Wang, L. Shao, D.E. Milkie, M.W. Davidson, C. Janetopoulos, X.S. Wu, J.A. Hammer, Z. Liu, B.P. English, Y. Mimori-Kiyosue, D.P. Romero, A.T. Ritter, J. Lippincott-Schwartz, L. Fritz-Laylin, R.D. Mullins, D.M. Mitchell, J.N. Bembenek, A.C. Reymann, R. Böhme, S.W. Grill, J.T. Wang, G. Seydoux, U.S. Tulu, D.P. Kiehart, E. Betzig, Lattice light-sheet microscopy: Imaging molecules to embryos at high spatiotemporal resolution, Science (80-. ). 346 (2014) 1257998. doi:10.1126/science.1257998.
[156] S.J. Sahl, F. Balzarotti, J. Keller-Findeisen, M. Leutenegger, V. Westphal, A. Egner, F. Lavoie-Cardinal, A. Chmyrov, T. Grotjohann, S. Jakobs, Comment on “Extended-resolution structured illumination imaging of endocytic and cytoskeletal dynamics,” Science. 352 (2016) 527. doi:10.1126/science.aad7983.
[157] L.H. Schaefer, D. Schuster, J. Schaffer, Structured illumination microscopy: Artefact analysis and reduction utilizing a parameter optimization approach, J. Microsc. 216 (2004) 165–174. doi:10.1111/j.0022-2720.2004.01411.x.
[158] G. Ball, J. Demmerle, R. Kaufmann, I. Davis, I.M. Dobbie, L. Schermelleh, SIMcheck: A toolbox for successful super-resolution structured illumination microscopy, Sci. Rep. 5 (2015) 15915. doi:10.1038/srep15915.
[159] M. Müller, V. Mönkemöller, S. Hennig, W. Hübner, T. Huser, Open-source image reconstruction of super-resolution structured illumination microscopy data in ImageJ, Nat. Commun. 7 (2016) 10980. doi:10.1038/ncomms10980.
[160] H. Blom, J. Widengren, Stimulated Emission Depletion Microscopy, Chem. Rev. 117 (2017) 7377–7427. doi:10.1021/acs.chemrev.6b00653.
[161] F. Göttfert, C.A. Wurm, V. Mueller, S. Berning, V.C. Cordes, A. Honigmann, S.W. Hell, Coaligned dual-channel STED nanoscopy and molecular diffusion analysis at 20 nm resolution, Biophys. J. 105 (2013) L01–L03. doi:10.1016/j.bpj.2013.05.029.
[162] G. Vicidomini, P. Bianchini, A. Diaspro, STED super-resolved microscopy, Nat. Methods. 15 (2018) 173–182. doi:10.1038/nmeth.4593.
[163] S.W. Hell, J. Wichmann, Breaking the diffraction resolution limit by stimulated emission: stimulated-emission-depletion fluorescence microscopy., Opt. Lett. 19 (1994) 780–2. doi:10.1364/OL.19.000780.
[164] R. Schmidt, C.A. Wurm, S. Jakobs, J. Engelhardt, A. Egner, S.W. Hell, Spherical nanosized focal spot unravels the interior of cells, Nat. Methods. 5 (2008) 539–544. doi:10.1038/nmeth.1214.
[165] J.M. Stern, J. Stanfield, Y. Lotan, S. Park, J.-T. Hsieh, J.A. Cadeddu, Efficacy of laser-activated gold nanoshells in ablating prostate cancer cells in vitro, J. Endourol. 21 (2007) 939–943. doi:10.1089/end.2007.0437.
[166] A.M. Alkilany, L.B. Thompson, S.P. Boulos, P.N. Sisco, C.J. Murphy, Gold nanorods: Their potential for photothermal therapeutics and drug delivery, tempered by the complexity of their biological interactions, Adv. Drug Deliv. Rev. 64 (2012) 190–199. doi:10.1016/j.addr.2011.03.005.
[167] W. Wegner, P. Ilgen, C. Gregor, J. Van Dort, A.C. Mott, H. Steffens, K.I. Willig, In vivo mouse and live cell STED microscopy of neuronal actin plasticity using far-red emitting fluorescent proteins, Sci. Rep. 7 (2017) 11781. doi:10.1038/s41598-017-11827-4.
[168] B. Hein, K.I. Willig, S.W. Hell, Stimulated emission depletion (STED) nanoscopy of a fluorescent protein-labeled organelle inside a living cell, Proc. Natl. Acad. Sci. 105 (2008) 14271–14276. doi:10.1073/pnas.0807705105.
[169] N.T. Urban, K.I. Willig, S.W. Hell, U.V. Nägerl, STED nanoscopy of actin dynamics in synapses deep inside living brain slices, Biophys. J. 101 (2011) 1277–1284.

doi:10.1016/j.bpj.2011.07.027.
[170] J. Heine, M. Reuss, B. Harke, E. D'Este, S.J. Sahl, S.W. Hell, Adaptive-illumination STED nanoscopy, Proc. Natl. Acad. Sci. 114 (2017) 201708304. doi:10.1073/pnas.1708304114.
[171] F. Göttfert, T. Pleiner, J. Heine, V. Westphal, D. Görlich, S.J. Sahl, S.W. Hell, Strong signal increase in STED fluorescence microscopy by imaging regions of subdiffraction extent, Proc. Natl. Acad. Sci. 114 (2017) 2125–2130. doi:10.1073/pnas.1621495114.
[172] S. Beater, P. Holzmeister, E. Pibiri, B. Lalkens, P. Tinnefeld, Choosing dyes for cw-STED nanoscopy using self-assembled nanorulers, Phys. Chem. Chem. Phys. 16 (2014) 6990–6996. doi:10.1039/c4cp00127c.
[173] Y.K. Tzeng, O. Faklaris, B.M. Chang, Y. Kuo, J.H. Hsu, H.C. Chang, Superresolution imaging of albumin-conjugated fluorescent nanodiamonds in cells by stimulated emission depletion, Angew. Chemie - Int. Ed. 50 (2011) 2262–2265. doi:10.1002/anie.201007215.
[174] G. Leménager, E. De Luca, Y.-P. Sun, P.P. Pompa, Super-resolution fluorescence imaging of biocompatible carbon dots, Nanoscale. 6 (2014) 8617. doi:10.1039/C4NR01970A.
[175] L. Shang, P. Gao, H. Wang, R. Popescu, D. Gerthsen, G.U. Nienhaus, Protein-based fluorescent nanoparticles for super-resolution STED imaging of live cells, Chem. Sci. 8 (2017) 2396–2400. doi:10.1039/c6sc04664a.
[176] H. Peuschel, T. Ruckelshausen, C. Cavelius, A. Kraegeloh, Quantification of internalized silica nanoparticles via STED microscopy, Biomed Res. Int. 2015 (2015) 1–16. doi:10.1155/2015/961208.
[177] S. Schubbe, C. Cavelius, C. Schumann, M. Koch, A. Kraegeloh, STED microscopy to monitor agglomeration of silica particles inside A549 cells, Adv. Eng. Mater. 12 (2010) 417–422. doi:10.1002/adem.201000093.
[178] S. Schübbe, C. Schumann, C. Cavelius, M. Koch, T. Müller, A. Kraegeloh, Size-dependent localization and quantitative evaluation of the intracellular migration of silica nanoparticles in Caco-2 cells, Chem. Mater. 24 (2012) 914–923. doi:10.1021/cm2018532.
[179] F.C. Chien, C.W. Kuo, Z.H. Yang, D.Y. Chueh, P. Chen, Exploring the formation of focal adhesions on patterned surfaces using super-resolution imaging, Small. 7 (2011) 2906–2913. doi:10.1002/smll.201100753.
[180] J.B. Pawley, Fundamental limits in confocal microscopy, in: Handb. Biol. Confocal Microsc. Third Ed., Springer US, Boston, MA, 2006: pp. 20–42. doi:10.1007/978-0-387-45524-2_2.
[181] V.E. Centonze, J.G. White, Multiphoton excitation provides optical sections from deeper within scattering specimens than confocal imaging, Biophys. J. 75 (1998) 2015–2024. doi:10.1016/S0006-3495(98)77643-X.
[182] I. Coto Hernández, M. Castello, L. Lanzanò, M. D'Amora, P. Bianchini, A. Diaspro, G. Vicidomini, Two-photon excitation STED microscopy with time-gated detection, Sci. Rep. 6 (2016) 19419. doi:10.1038/srep19419.
[183] A. Doi, R. Oketani, Y. Nawa, K. Fujita, High-resolution imaging in two-photon excitation microscopy using in situ estimations of the point spread function., Biomed. Opt. Express. 9 (2018) 202–213. doi:10.1364/BOE.9.000202.
[184] P. Bethge, R. Chéreau, E. Avignone, G. Marsicano, U.V. Nägerl, Two-photon excitation STED microscopy in two colors in acute brain slices, Biophys. J. 104 (2013) 778–785. doi:10.1016/j.bpj.2012.12.054.
[185] K.T. Takasaki, J.B. Ding, B.L. Sabatini, Live-cell superresolution imaging by pulsed STED two-photon excitation microscopy, Biophys. J. 104 (2013) 770–777. doi:10.1016/j.bpj.2012.12.053.
[186] M. Dai, R. Jungmann, P. Yin, Optical imaging of individual biomolecules in densely packed clusters, Nat. Nanotechnol. 11 (2016) 798–807. doi:10.1038/nnano.2016.95.
[187] F. Balzarotti, Y. Eilers, K.C. Gwosch, A.H. Gynnå, V. Westphal, F.D. Stefani, J. Elf, S.W. Hell, Nanometer resolution imaging and tracking of fluorescent molecules with minimal photon fluxes, Science (80-. ). 355 (2017) 606–612. doi:10.1126/science.aak9913.
[188] A. Trache, G.A. Meininger, Total Internal Reflection Fluorescence (TIRF) microscopy, in: Curr. Protoc. Microbiol., John Wiley & Sons, Inc., Hoboken, NJ, USA, 2008: p. Unit12.18.

doi:10.1002/9780471729259.mc02a02s10.
[189] S.T. Hess, T.P.K. Girirajan, M.D. Mason, Ultra-high resolution imaging by fluorescence photoactivation localization microscopy, Biophys. J. 91 (2006) 4258–4272. doi:10.1529/biophysj.106.091116.
[190] M.J. Rust, M. Bates, X. Zhuang, Sub-diffraction-limit imaging by stochastic optical reconstruction microscopy (STORM), Nat. Methods. 3 (2006) 793–795. doi:10.1038/nmeth929.
[191] U. Endesfelder, M. Heilemann, Direct Stochastic Optical Reconstruction Microscopy (dSTORM), in: Methods Mol. Biol., 2015: pp. 263–276. doi:10.1007/978-1-4939-2080-8_14.
[192] J. Lippincott-Schwartz, G.H. Patterson, Photoactivatable fluorescent proteins for diffraction-limited and super-resolution imaging, Trends Cell Biol. 19 (2009) 555–565. doi:10.1016/j.tcb.2009.09.003.
[193] D.R. Whelan, T.D.M. Bell, Image artifacts in single molecule localization microscopy: Why optimization of sample preparation protocols matters, Sci. Rep. 5 (2015) 7924. doi:10.1038/srep07924.
[194] G.T. Dempsey, J.C. Vaughan, K.H. Chen, M. Bates, X. Zhuang, Evaluation of fluorophores for optimal performance in localization-based super-resolution imaging, Nat. Methods. 8 (2011) 1027–1036. doi:10.1038/nmeth.1768.
[195] A. Jimenez, K. Friedl, C. Leterrier, About samples, giving examples: Optimized Single Molecule Localization Microscopy, Methods. (2019). doi:10.1016/j.ymeth.2019.05.008.
[196] D.J. Nieves, K. Gaus, M.A.B. Baker, DNA-based super-resolution microscopy: DNA-PAINT, Genes (Basel). 9 (2018) 621. doi:10.3390/genes9120621.
[197] S.A. Jones, S.H. Shim, J. He, X. Zhuang, Fast, three-dimensional super-resolution imaging of live cells, Nat. Methods. 8 (2011) 499–505. doi:10.1038/nmeth.1605.
[198] M. Bates, G.T. Dempsey, K.H. Chen, X. Zhuang, Multicolor super-resolution fluorescence imaging via multi-parameter fluorophore detection, ChemPhysChem. 13 (2012) 99–107. doi:10.1002/cphc.201100735.
[199] A. Fernandez, M. Bautista, R. Stanciauskas, T. Chung, F. Pinaud, Cell-shaping micropatterns for quantitative super-resolution microscopy imaging of membrane mechanosensing proteins, ACS Appl. Mater. Interfaces. 9 (2017) 27575–27586. doi:10.1021/acsami.7b09743.
[200] S. Nie, Editorial: Understanding and overcoming major barriers in cancer nanomedicine, Nanomedicine. 5 (2010) 523–528. doi:10.2217/nnm.10.23.
[201] P. Foroozandeh, A.A. Aziz, Insight into Cellular Uptake and Intracellular Trafficking of Nanoparticles., Nanoscale Res. Lett. 13 (2018) 339. doi:10.1186/s11671-018-2728-6.
[202] S. De Koker, J. Cui, N. Vanparijs, L. Albertazzi, J. Grooten, F. Caruso, B.G. De Geest, Engineering polymer hydrogel nanoparticles for lymph node-targeted delivery, Angew. Chemie - Int. Ed. 55 (2016) 1334–1339. doi:10.1002/anie.201508626.
[203] D. Van Der Zwaag, N. Vanparijs, S. Wijnands, R. De Rycke, B.G. De Geest, L. Albertazzi, Super resolution imaging of nanoparticles cellular uptake and trafficking, ACS Appl. Mater. Interfaces. 8 (2016) 6391–6399. doi:10.1021/acsami.6b00811.
[204] Y. Li, L. Shang, G.U. Nienhaus, Super-resolution imaging-based single particle tracking reveals dynamics of nanoparticle internalization by live cells., Nanoscale. 8 (2016) 7423–9. doi:10.1039/c6nr01495j.
[205] A. Ardizzone, S. Kurhuzenkau, S. Illa-Tuset, J. Faraudo, M. Bondar, D. Hagan, E.W. Van Stryland, A. Painelli, C. Sissa, N. Feiner, L. Albertazzi, J. Veciana, N. Ventosa, Nanostructuring lipophilic dyes in water using stable vesicles, quatsomes, as scaffolds and their use as probes for bioimaging, Small. 14 (2018) 1703851. doi:10.1002/smll.201703851.
[206] R. Roy, S. Hohng, T. Ha, A practical guide to single-molecule FRET, Nat. Methods. 5 (2008) 507–516. doi:10.1038/nmeth.1208.
[207] N.D. Huebsch, D.J. Mooney, Fluorescent resonance energy transfer: A tool for probing molecular cell-biomaterial interactions in three dimensions, Biomaterials. 28 (2007) 2424–2437. doi:10.1016/j.biomaterials.2007.01.023.

[208] P.A. Santi, Light Sheet Fluorescence Microscopy, J. Histochem. Cytochem. 59 (2011) 129–138. doi:10.1369/0022155410394857.
[209] J.M. Girkin, M.T. Carvalho, The light-sheet microscopy revolution, J. Opt. (United Kingdom). 20 (2018) 053002. doi:10.1088/2040-8986/aab58a.
[210] T.-L. Liu, S. Upadhyayula, D.E. Milkie, V. Singh, K. Wang, I.A. Swinburne, K.R. Mosaliganti, Z.M. Collins, T.W. Hiscock, J. Shea, A.Q. Kohrman, T.N. Medwig, D. Dambournet, R. Forster, B. Cunniff, Y. Ruan, H. Yashiro, S. Scholpp, E.M. Meyerowitz, D. Hockemeyer, D.G. Drubin, B.L. Martin, D.Q. Matus, M. Koyama, S.G. Megason, T. Kirchhausen, E. Betzig, Observing the cell in its native state: Imaging subcellular dynamics in multicellular organisms, Science (80-. ). 360 (2018) eaaq1392. doi:10.1126/science.aaq1392.
[211] T. Ando, S.P. Bhamidimarri, N. Brending, H. Colin-York, L. Collinson, N. De Jonge, P.J. de Pablo, E. Debroye, C. Eggeling, C. Franck, M. Fritzsche, H. Gerritsen, B.N.G. Giepmans, K. Grunewald, J. Hofkens, J.P. Hoogenboom, K.P.F. Janssen, R. Kaufmann, J. Klumperman, N. Kurniawan, J. Kusch, N. Liv, V. Parekh, D.B. Peckys, F. Rehfeldt, D.C. Reutens, M.B.J. Roeffaers, T. Salditt, I.A.T. Schaap, U.S. Schwarz, P. Verkade, M.W. Vogel, R. Wagner, M. Winterhalter, H. Yuan, G. Zifarelli, The 2018 correlative microscopy techniques roadmap, J. Phys. D. Appl. Phys. 51 (2018) 443001. doi:10.1088/1361-6463/aad055.
[212] S.W. Hell, S.J. Sahl, M. Bates, X. Zhuang, R. Heintzmann, M.J. Booth, J. Bewersdorf, G. Shtengel, H. Hess, P. Tinnefeld, A. Honigmann, S. Jakobs, I. Testa, L. Cognet, B. Lounis, H. Ewers, S.J. Davis, C. Eggeling, D. Klenerman, K.I. Willig, G. Vicidomini, M. Castello, A. Diaspro, T. Cordes, The 2015 super-resolution microscopy roadmap, J. Phys. D. Appl. Phys. 48 (2015) 443001. doi:10.1088/0022-3727/48/44/443001.
[213] M. Hauser, M. Wojcik, D. Kim, M. Mahmoudi, W. Li, K. Xu, Correlative super-resolution microscopy: New dimensions and new opportunities, Chem. Rev. 117 (2017) 7428–7456. doi:10.1021/acs.chemrev.6b00604.
[214] M.G. Paez-Segala, M.G. Sun, G. Shtengel, S. Viswanathan, M.A. Baird, J.J. Macklin, R. Patel, J.R. Allen, E.S. Howe, G. Piszczek, H.F. Hess, M.W. Davidson, Y. Wang, L.L. Looger, Fixation-resistant photoactivatable fluorescent proteins for CLEM, Nat. Methods. 12 (2015) 215–218. doi:10.1038/nmeth.3225.
[215] E. Johnson, E. Seiradake, E.Y. Jones, I. Davis, K. Grünewald, R. Kaufmann, Correlative in-resin super-resolution and electron microscopy using standard fluorescent proteins, Sci. Rep. 5 (2015) 9583. doi:10.1038/srep09583.
[216] M. Wojcik, M. Hauser, W. Li, S. Moon, K. Xu, Graphene-enabled electron microscopy and correlated super-resolution microscopy of wet cells, Nat. Commun. 6 (2015) 7384. doi:10.1038/ncomms8384.
[217] M.W. Tuijtel, A.J. Koster, S. Jakobs, F.G.A. Faas, T.H. Sharp, Correlative cryo super-resolution light and electron microscopy on mammalian cells using fluorescent proteins, Sci. Rep. 9 (2019) 1369. doi:10.1038/s41598-018-37728-8.
[218] G. Wolff, C. Hagen, K. Grünewald, R. Kaufmann, Towards correlative super-resolution fluorescence and electron cryo-microscopy, Biol. Cell. 108 (2016) 245–258. doi:10.1111/boc.201600008.
[219] S. Kobayashi, M. Iwamoto, T. Haraguchi, Live correlative light-electron microscopy to observe molecular dynamics in high resolution, Microscopy. 65 (2016) 296–308. doi:10.1093/jmicro/dfw024.
[220] M. Bates, B. Huang, G.T. Dempsey, X. Zhuang, Multicolor super-resolution imaging with photo-switchable fluorescent probes, Science (80-. ). 317 (2007) 1749–1753. doi:10.1126/science.1146598.
[221] J. Bückers, D. Wildanger, S.W. Hell, G. Vicidomini, L. Kastrup, Simultaneous multi-lifetime multi-color STED imaging for colocalization analyses, Opt. Express. 19 (2011) 3130. doi:10.1364/oe.19.003130.
[222] S. Waldchen, J. Lehmann, T. Klein, S. Van De Linde, M. Sauer, Light-induced cell damage in live-cell super-resolution microscopy, Sci. Rep. 5 (2015) 15348. doi:10.1038/srep15348.